

MONTHLY WEATHER REVIEW

VOLUME 94, NUMBER 7

JULY 1966

FRICIONAL AND THERMAL INFLUENCES IN THE SOLAR SEMIDIURNAL TIDE

MILES F. HARRIS, FREDERICK G. FINGER, AND SIDNEY TEWELES

Environmental Science Services Administration, Washington, D.C.

ABSTRACT

The frictional and thermal contributions to $S^2_{2,2}(p)$, the dominant wave type in the progressive solar semidiurnal pressure wave, are evaluated from upper air observations at nine rawinsonde stations. The theoretical basis for the investigation follows from the approximation of friction as a potential force in the tidal equations. The model parameters and boundary conditions are those adopted by Siebert. Surface friction is evaluated semi-empirically, by the use of a friction model which is essentially an adaptation, to the semidiurnal motions, of the Ekman theory of the boundary layer. The assumption of a constant coefficient of the vertical transfer of momentum leads to uncertainties in the magnitude of the frictional contribution to the wave.

Further uncertainties arise from a systematic error in the observed temperatures, caused by radiation effects on the radiosonde instrument. The latter error, however, is believed to be negligible in the lower troposphere, where an unexpectedly large temperature variation is apparently caused by eddy transfer of heat from the earth's surface.

The results of the study must be considered in the light of the probable errors arising from data sampling, from the diurnal bias in the radiosonde observations, and from the restrictive assumptions of the theory. Considered in this light, the results suggest that the semidiurnal oscillation may be explained by three processes, of approximately equal importance: (1) eddy transfer of heat from the earth's surface; (2) direct absorption of solar radiation by water vapor and ozone, as computed by Siebert; and (3) surface friction, or eddy transfer of momentum. Surface friction apparently delays the surface pressure oscillation by about one hour.

1. INTRODUCTION

The classical theory of the atmospheric tides explains the prominent semidiurnal oscillation in surface pressure as the result of strong resonance amplification of very small oscillations due to surface heating and to the gravitational tidal force of the sun. In recent years, a number of investigators have abandoned the resonance theory as untenable in the light of rocketsonde measurements of the thermal structure of the upper stratosphere and lower mesosphere. Haurwitz [10], in a survey of present knowledge about the tides, has summarized the reasons for the current viewpoint. The evidence currently points to relatively small magnification of the equilibrium tides (of the order of $\times 3$ or $\times 4$ instead of $\times 100$), and to direct absorption of solar radiation by water vapor [13] and ozone [13], [1] as the main cause of the pressure wave. Thus, temperature changes involving essentially the total mass of the atmosphere, in contrast to a relatively thin boundary layer affected by eddy con-

duction of heat from the earth's surface, are believed to account for the large amplitude and nearly constant phase of the solar semidiurnal tide.

On the basis of the distribution of water vapor, Siebert [13] (all future references to Siebert are to [13]) calculated the temperature oscillation in the troposphere resulting from insolation. His estimate of its amplitude and phase [$3.11 \times 10^{-2} \text{C.}^\circ$, 0300 (1500)] yielded a surface pressure oscillation of amplitude 0.36 mb. and phase 0900 (2100). The amplitude and phase of the observed oscillation are quoted by Siebert as 1.19 mb., 0948 (2148). He estimated that an additional 0.10 mb. or more might be accounted for by temperature changes in the ozone-sphere (See also [1], [5].) but concluded that eddy transfer of heat from the surface is negligible, in comparison with direct absorption of energy, as a tide-producing force. Siebert attributed to surface friction the phase retardation of the observed over the theoretically derived tide, pointing out that the lunar tidal phase lags the theoret-

ical phase (known exactly in this case) by 36 min. However, because he had accounted for little more than a third of the amplitude of the observed variation, Siebert concluded that a completely satisfactory explanation of the semidiurnal wave does not yet exist, perhaps because the empirical data used for determining the thermal action are not sufficiently reliable. Butler and Small [1] and Green [5] have suggested that ozone heating accounts for the unexplained component of the tide.

Since the publication of Siebert's results, we have obtained additional empirical data in the form of the diurnal and semidiurnal variations of temperature, wind, and height of isobaric surfaces at nine rawinsonde stations in the Northern Hemisphere. Analysis of the semidiurnal results, to determine whether they are consistent with current views on the origin of the tide, suggested itself as an interesting possibility. In particular, we were interested in accounting for the phase retardation of the observed over the theoretical pressure oscillation, which Siebert explained as the result of surface friction. Using the observations for four of the lower-latitude stations shown in table 3, Appendix B, Harris [7] showed that surface friction advances rather than retards the phase of the semidiurnal wind in the friction layer, as compared with the phase of the wind due to pressure forces, and speculated that friction might act to advance rather than retard the pressure wave. This inference, as the present study shows, proved to be wrong.

The data also presented an opportunity to reexamine, in the light of actual observations, the magnitude of the thermal contribution to the atmospheric tide. An element of uncertainty is introduced into this phase of the investigation by a well-recognized diurnal bias in the observed temperatures, caused by radiation effects on the radiosonde sensor. Since the semidiurnal component of this systematic error is not known, its effect on the computations is difficult to estimate. The error is probably small or non-existent in the lowest two or three kilometers of the atmosphere. Here, the temperature variation apparently caused by eddy transfer of heat from the earth's surface turned out to be unexpectedly large, sufficient to account for the unexplained component of the thermal tide.

The study also gives a quantitative, though admittedly uncertain, value to the retarding effect of surface friction on the pressure oscillation. Thus, eddy transfer of heat and momentum, combined with the direct absorption of energy by water vapor and ozone as computed by Siebert, appears to explain the pressure oscillation. The three processes appear to be of approximately equal importance.

The purpose of this article is to document the results summarized above. Section 2 describes the theoretical approach. Since the inclusion of frictional terms in the equations of motion involves no departure from the basic theory, details of the derivation are consigned to Appendix A. Section 3 describes the analysis of the upper-air data and the computation of the diabatic tem-

perature variation, and Appendix B presents the analyzed data. In section 4, and Appendix C, the theoretical basis for the computation of frictional forces is described. The frictional model is essentially an extension, to the semidiurnal motions, of the Ekman theory of the boundary layer. Sections 5 and 6 describe the numerical computations and attempt to evaluate the results.

2. THEORETICAL APPROACH

The approach follows closely that of Siebert, which has evolved from the work of many investigators from Laplace onward. The theory assumes that the tidal changes may be regarded as small perturbations superimposed on an otherwise undisturbed atmosphere. The undisturbed atmosphere is described by the static pressure, the density, and the temperature, and these are assumed to vary with height z but not with colatitude θ and longitude ϕ . The usual assumptions of perturbation theory lead to a set of linearized equations: the equations of motion and state, the hydrostatic equation, the equation of continuity, and the first law of thermodynamics. Since the variations are periodic, the perturbation quantities are set proportional to $\exp[i\sigma t]$, $\sigma = 2\omega f$, where ω is the angular velocity of the earth, and $2f$ is the frequency of the oscillation. To these usual assumptions we add another: namely, that the vertical flux of momentum can be considered a potential force, so that

$$\frac{\partial \delta \tau_{\theta}}{\partial z} = -\frac{1}{a} \frac{\partial}{\partial \theta} \left(\frac{\partial \delta \tau}{\partial z} \right), \quad \frac{\partial \delta \tau_{\phi}}{\partial z} = -\frac{1}{a \sin \theta} \frac{\partial}{\partial \phi} \left(\frac{\partial \delta \tau}{\partial z} \right). \quad (1)$$

The validity of this assumption will be examined in section 4, where the variation of the frictional force with colatitude is considered.

Manipulation of the basic equations leads to a partial differential equation in the divergence, $\chi(\theta, \phi, z, t)$, equation (44) in Appendix A. Further references to equations in this section, except where noted otherwise, will be to the equations in Appendix A. Equation (44) is solved by the method of separation of variables, after representing χ and the other variables by series expansions in terms of the eigenfunctions $\psi_n(\theta, \phi)$ of the operator F , defined by (38). With the constant of separation denoted by $1/h_n$, two ordinary differential equations are obtained, (46) and (47). The first of these becomes the basis for determining the values of h_n appropriate to each wave type $S_{\lambda, n}^s$, where λ indicates the frequency, s the periodicity in ϕ , and n the wave type when Hough's functions are used. Although analogous to the ocean depth in the theory of ocean tides, the h_n 's are in a mathematical sense eigenvalues of the differential equation (46), and may even take on negative values. In Siebert's terminology, h_n is the *equivalent depth*. For wave type $S_{2,2}^2$, the dominant component of the semidiurnal migrating wave, h_n has the value 7.85 km. It is this wave type that we shall investigate.

Further manipulation of the equations, and a trans-

formation of variables, lead to the solutions given by equations (53) to (58). For a lower boundary condition, Siebert makes the usual assumption that the vertical component of the velocity vanishes at the earth's surface. As an upper boundary condition, he requires that the kinetic energy per column of unit cross-section be finite, equation (60). The specification of a model atmosphere described by the distribution of the scale height H , together with these boundary conditions, leads eventually to equations for the components of motion, the pressure, and the temperature, in terms of the forcing functions: gravitational potential, diabatic temperature variation expressed as a potential, and friction approximated as a potential force.

Since the pressure variation at the ground is the best observed data associated with the atmospheric tides, this is the quantity ordinarily used to test theoretical models. Equation (74), the basis for numerical calculations in section 4, is reproduced here:

$$S_{2,2}^2(p) = M_2 \left[\overline{\delta p(0)} + \frac{a \sin \theta}{2h_2} i \delta \tau_{\phi,2}(0) - \frac{p_0(0)}{T_0(0)} \int_{x_1}^{x_2} \delta T_{d,2}(x) y_2^0(x) e^{-x/2} dx \right]. \quad (2)$$

In this equation, $S_{2,2}^2(p)$ is the surface pressure variation associated with the dominant wave type in the semidiurnal migrating wave. M is a "magnification factor," a function of the model atmosphere and the equivalent depth. The first term in the brackets represents the equilibrium value of the gravitational tide at the earth's surface. The gravitational tide has been explained by Siebert, so it will not be considered in this study. The second term in the brackets is the component of the surface stress directed along the parallels, and the final term is the integral of the diabatic temperature variation in the layer of interest, weighted by the appropriate factor depending on the distribution of H and on h_n . The variable x represents a modified height coordinate and is a function of the scale height.

For details leading to the derivation of equation (2) above, the reader is referred to Appendix A.

3. DATA

The computation of the semidiurnal variations in pressure, temperature, and wind above the surface is limited to those rawinsonde stations which took four observations daily, prior to and after the change in the scheduled time of observations in mid-1957. This change effectively increased the number of observations in the combined series from four to eight. The method of combining the data, applied earlier to stratospheric observations by Johnson [12] and its justification were described by Harris [6].

Table 3 in Appendix B presents the results of the diurnal and semidiurnal computations for the nine stations, together with the probable errors calculated according to

the method outlined by Chapman [2]. The stations were selected to give as wide a latitudinal distribution of the semidiurnal changes as possible, but unfortunately the available observations are concentrated at middle latitudes. Examination of the probable errors reveals that the determinations, particularly those of the temperature variation, being based on only two years' data, are far from satisfactory. Nevertheless, they undoubtedly do give a gross indication of the semidiurnal changes and some evidence of their geographical distribution. The wind components in the tabulated data follow the convention used in meteorology, that is, the phase angles apply to eastward and poleward (rather than equatorward) components of the wind. The phase angles have been corrected to allow for the estimated actual release time, which differs from the scheduled time of observation, and for the ascent time of the balloon.

The semidiurnal variation S_2 includes not only a westward moving, progressive wave but also a standing wave, sometimes called the *polar vibration*, which has been studied extensively by Haurwitz [11], [9]. The standing wave S_2^0 is proportionately large (compared with S_2^2) at high latitudes. Since our theoretical results apply only to $S_{2,2}^2$, it would be desirable to separate the various wave types for the purpose of our study. Unfortunately, the observation points are far too few to render any such attempt successful. We shall therefore rely for verification of the theory mainly on the stations between 30° and 40° latitude; and of these, on the four of the five stations which give fairly homogeneous results. The data for Fort Worth appear to be anomalous in a number of respects. Of the four stations we shall examine closely, two (Bermuda and the Azores) are ocean stations and two (Valparaiso and Osan) are coastal stations, and for these the data appear to be relatively homogeneous.

In addition to the large random errors in the data, the temperature and hence the height variations probably contain a bias resulting from radiation effects on the radiosonde temperature sensor. This error is believed to be most pronounced in the stratosphere, where there is evidence that it is rather large in the case of the 24-hr. component [8], [4]. An estimate of the error has been obtained by treating the diurnal and semidiurnal changes as the result of simple progressive waves, neglecting friction, and using the observed winds to compute estimates of the pressure variation. The amplitudes and phases of the diurnal and semidiurnal height changes found in this way are presented in table 4, Appendix B. The computed semidiurnal height variations are rather irregular, and therefore the semidiurnal error in the temperature cannot be estimated with much confidence. However, in interpreting the results of this investigation, it is assumed that the computations involving the temperature contain an error, of undetermined magnitude, resulting from this systematic radiation effect.

In order to determine the surface pressure variation from the observational data, we need to compute the

stress $\delta\tau_\phi(0)$ and the diabatic temperature variation, as well as (for comparison) the stress component $\delta\tau_\theta(0)$. The diabatic temperature variation and the latitudinal component of the surface stress, $\delta\tau_\phi(0)$, are to be inserted in equation (2).

From equations (20), (23), and (29) in Appendix A, we can closely approximate the diabatic temperature variation in terms of the height variation:

$$\delta T_d \sim \frac{g(\delta z_2 - \delta z_1)}{R \ln[p_0(z_1)/p_0(z_2)]} - \frac{\kappa g(\delta z_1 + \delta z_2)}{2R} \quad (3)$$

where δT_d is the value at the middle of the layer bounded by z_1 and z_2 . For this purpose the height values were very slightly smoothed where obvious errors occurred. The values of δT_d obtained in this way are shown in table 1. The thickness was used to evaluate the temperature variation since the actual values in Appendix B contain large random errors.

An adequate determination of the components of the surface stress presented greater difficulty. Although the components of friction can be computed as residual values in the horizontal equations of motion, and these residual values integrated with respect to height to obtain the surface stress components, this computation produced values of the stress which appear to be unrealistically large, ranging from about 0.4 to 2.5 dynes cm^{-2} . This result was not unexpected, since it is intuitively evident that the differences of vector quantities containing random errors are likely to be larger than the true residuals. We therefore resorted to a theoretical model to compute the surface stress.

4. FRICTION IN THE SEMIDIURNAL TIDE

On the assumption that the contribution of the pressure gradient force to the semidiurnal wind does not vary with height, Harris [7] showed that a solution for the frictional components of the wind is

$$v_f = A e^{-bz} \sin(2\omega t + \alpha - bz) \quad (4)$$

$$u_f = -B e^{-bz} \cos(2\omega t + \alpha - bz). \quad (5)$$

For a more complete derivation of the friction model, outlined here, the reader is referred to Appendix C. The coefficient of the eddy exchange of momentum K_m is assumed to be invariant with time and height. The earlier solution required the amplitudes of the components of the pressure-related wind, U_p and V_p to be equal. Further examination has shown that this condition may be replaced by one less restrictive (Appendix C). We find instead that when

$$b = \left(\frac{\omega}{K_m}\right)^{1/2} \left(\frac{A}{A+B \cos \theta}\right)^{1/2} \sin \theta \quad (6)$$

the required condition is that

$$\left(\frac{U_p}{U_p + V_p \cos \theta}\right)^{1/2} = \left(\frac{V_p}{V_p + U_p \cos \theta}\right)^{1/2} \quad (7)$$

TABLE 1.—Amplitude (A , 10^{-3} °C.) and phase (α , deg.) of mean diabatic temperature variation in 50-mb. layers, July 1956 to June 1958.

p_0 (mb.)	Valparaiso		Bermuda		Fort Worth		Osan		Azores	
	A	α	A	α	A	α	A	α	A	α
975-----	436	43	107	34	748	14	382	35	150	33
925-----	220	35	94	30	432	359	212	31	134	44
875-----	95	16	129	19	332	343	78	47	126	40
825-----	116	357	82	31	213	5	51	0	104	39
775-----	57	349	86	32	184	21	29	344	94	35
725-----	59	24	75	20	113	7	37	294	82	44
675-----	47	52	73	44	106	5	32	42	47	35
625-----	47	46	82	45	97	342	46	76	47	23
575-----	75	20	89	56	63	356	45	67	92	359
525-----	63	20	55	45	58	325	44	75	142	356
475-----	57	14	33	23	56	308	56	75	152	353
425-----	54	3	45	44	69	325	47	15	104	349
375-----	45	14	35	25	83	327	39	85	81	340
325-----	32	358	37	6	75	351	36	64	57	349
275-----	45	318	37	8	73	28	56	98	47	47
225-----	47	290	49	20	66	30	59	101	40	49
175-----	4	284	65	41	95	59	47	101	45	65
125-----	27	180	35	146	79	310	15	143	48	68
75-----	17	190	6	84	152	268	31	0	68	123

p_0 (mb.)	Sault Ste. Marie		Stephenville		Keflavik		Thule		A	α
	A	α	A	α	A	α	A	α		
975-----	409	45	241	78	111	22	46	352		
925-----	235	41	178	84	15	233	94	1		
875-----	103	40	118	35	28	205	5	11		
825-----	68	47	75	85	30	203	5	180		
775-----	35	45	39	72	28	250	5	158		
725-----	44	55	20	63	24	237	29	346		
675-----	35	24	5	37	20	232	24	5		
625-----	30	7	32	347	22	257	14	8		
575-----	33	5	20	339	32	242	22	5		
525-----	46	356	57	23	24	225	22	5		
475-----	71	63	91	27	22	248	26	4		
425-----	81	64	109	30	9	201	36	358		
375-----	58	65	106	24	17	29	46	356		
325-----	44	58	32	73	32	46	39	347		
275-----	20	53	24	122	46	50	24	324		
225-----	4	135	28	169	51	47	8	277		
175-----	48	101	103	106	52	43	26	246		
125-----	44	103	71	116	50	16	14	143		
75-----	40	162	58	123	53	359	57	98		

Figure 1 shows that equation (7) is a fairly close approximation to actuality, certainly better than the condition $U_p = V_p$ required in the earlier solution. The values of U_p and V_p used in (7) were estimated by combining the continuity equation and the vorticity equation found by cross-differentiation of the component equations of motion. In this way, v can be eliminated, and integration of the resulting equation with respect to height gives $\bar{u}(\theta)$ as a function of $\delta p(0)(\theta)$ when the boundary conditions are $\rho_0 w = 0$ at $z = 0$ and $z = \infty$. The equation in $\bar{u}(\theta)$ can then be solved by the method of variation of parameters with the condition that $\bar{u} = 0$ at $\theta = 0$, and $\bar{v}(\theta)$ found by substituting $\bar{u}(\theta)$ into the continuity equation. The resulting values of u and v , assuming $\delta p(0) \propto 1.20 \sin^3 \theta$ mb., are graphed in figures 2 and 3. Since the integrated frictional effect is small, we assume that $U_p \approx \bar{u}$ and $V_p \approx \bar{v}$. The observed mean values of u and v , with respect to pressure, are shown for comparison.

The revised solution leads to expressions for the surface stress, in terms of the depth of the frictional layer h , and the angle D which the semidiurnal wind at the lower boundary makes with the wind as a result of pressure gradient forces alone. The components of the surface stress become

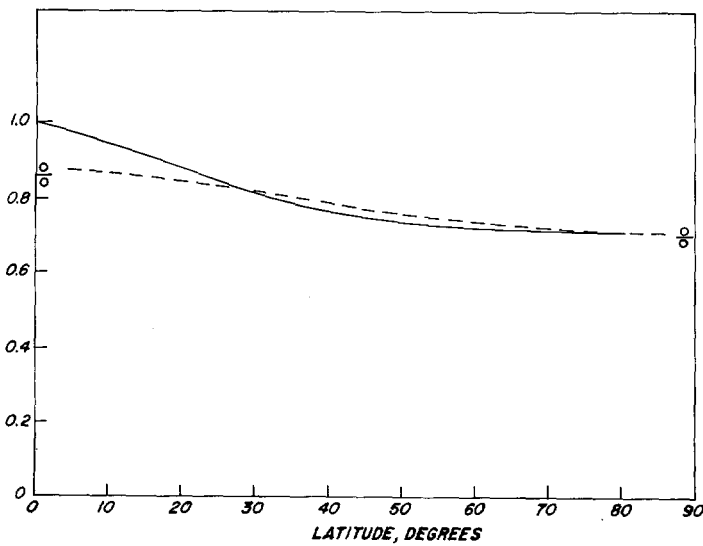


FIGURE 1.—Approximate equality of $[V_p/(V_p + U_p \cos \theta)]^{1/2}$; shown by the solid curve, and $[U_p/(U_p + V_p \cos \theta)]^{1/2}$, shown as the dashed curve. The solution for the frictional components of the wind implies the equality of these quantities.

$$\delta\tau_\phi(0) = 8\rho_0\omega \frac{V_p^2 \sin^2 \theta}{V_p + U_p \cos \theta} \frac{h \sin D}{3\pi + 4D} \sin(2\omega t + \beta + D) \quad (8)$$

$$\delta\tau_\theta(0) = -8\rho_0\omega \frac{U_p^2 \sin^2 \theta}{U_p + V_p \cos \theta} \frac{h \sin D}{3\pi + 4D} \cos(2\omega t + \beta + D) \quad (9)$$

where β is the phase angle of the surface pressure oscillation, plus 180° . Figure 4 shows the variation with latitude of the coefficients of $h \sin \alpha_0 D / (3\pi + 4D)$ in the two equations.

The condition that friction be a potential force,

$$\frac{\partial}{\partial \phi} [\delta\tau_\theta(0)] = \frac{\partial}{\partial \theta} [\sin \theta \delta\tau_\phi(0)],$$

implies that

$$\frac{2U_p^2 \sin^2 \theta}{U_p + V_p \cos \theta} = \frac{\partial}{\partial \theta} \left(\frac{V_p^2 \sin^3 \theta}{V_p + U_p \cos \theta} \right) \quad (10)$$

if h and D are assumed to be independent of latitude. The two sides of equation (10) were compared by evaluating the indicated functions of U_p and V_p , approximating the derivative by finite differences taken over increments of 10° of latitude. The comparison, shown in figure 5, indicates that the assumption of friction as a potential force is a reasonable first approximation, for the semidiurnal motions. If h is assumed to vary as $\sin \theta$, the agreement between the resulting functions is about the same as that shown by the curves in figure 5.

An independently derived value of the surface stress is available from the work of Estoque [3] who devised a numerical model of the diurnal variations in the boundary

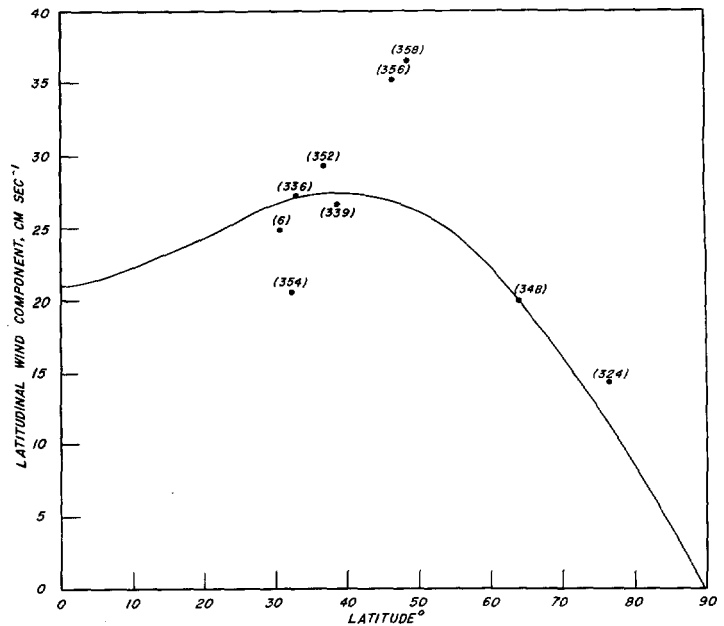


FIGURE 2.—Comparison of the mean eastward component of the semidiurnal wind in the layer represented by the observations (table 3) with the empirically derived component \bar{v} , which has the constant phase angle 338° . The observed phase angle at each of the stations is indicated in parentheses.

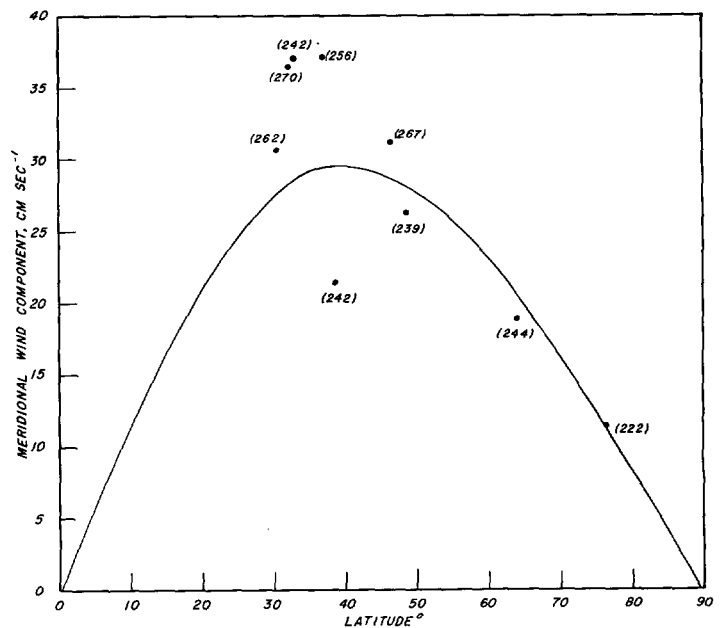


FIGURE 3.—Comparison of the mean equatorward component of the semidiurnal wind in the layer represented by the observations (table 3) with the empirically derived component \bar{u} , which has the constant phase angle 248° . The observed phase angle at each of the stations is indicated in parentheses.

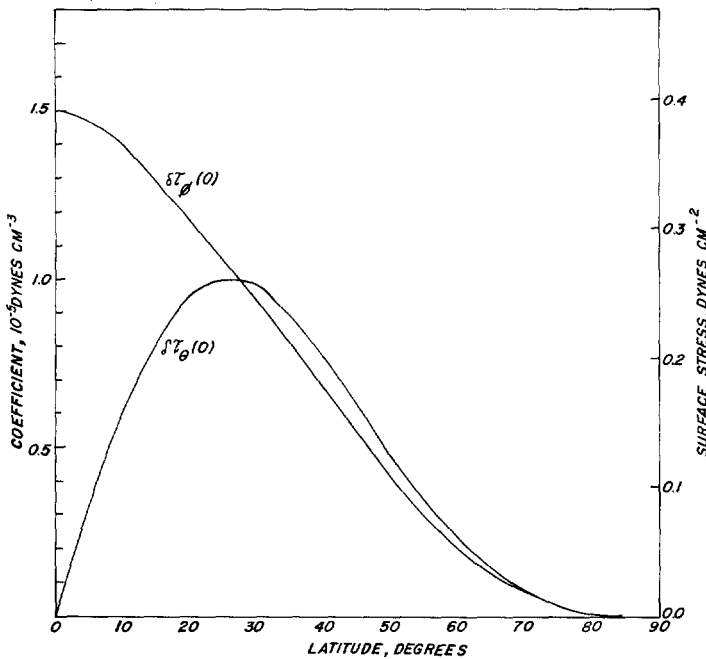


FIGURE 4.—Variation with latitude of the coefficients of $h \sin \alpha_0 / (3\pi + 4D)$ in equations (8) for $\delta\tau_\phi(0)$ and (9) for $\delta\tau_\theta(0)$; scale at left. Variation with latitude of the latitudinal component of the surface stress, $\delta\tau_\phi(0)$, and the meridional component, $\delta\tau_\theta(0)$, when h and D are 6 km. and 30° , respectively; scale at right.

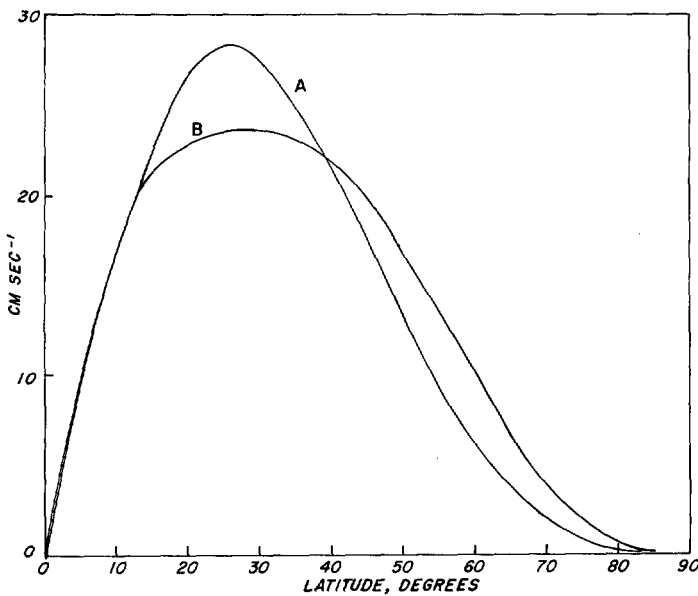


FIGURE 5.—Comparison between the derivatives $b(\partial/\partial\phi)[\delta\tau_\theta(0)]$, indicated by curve (A), and $b(\partial/\partial\theta)[\sin\theta\delta\tau_\phi(0)]$, indicated by curve (B). Equality of curves A and B implies that friction is a potential force, provided the coefficient of momentum transfer, K_m , is constant with latitude.

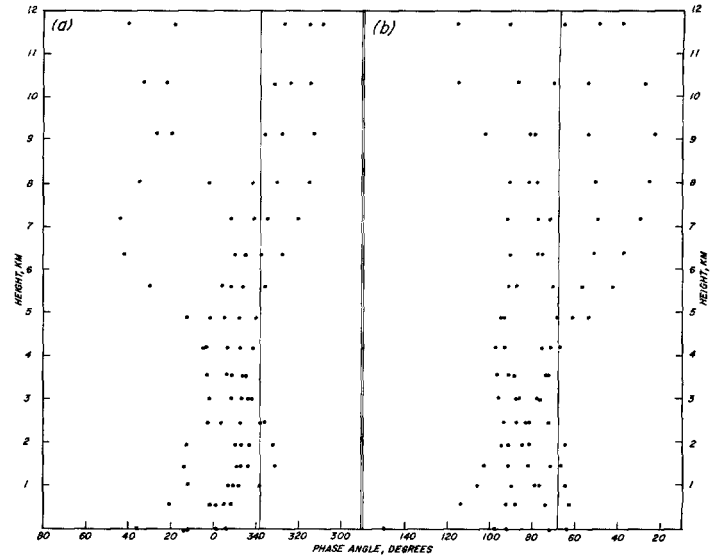


FIGURE 6.—Variation with height of the phase angle of v , the eastward component of the semidiurnal wind, at five stations between latitudes 30° and 40° (table 3, Appendix B), is shown in (a). The variation with height of the phase angle of $-u$, the poleward velocity component, is shown in (b). The vertical lines indicate the phase angles of the wind component due to pressure-gradient forces alone, assumed constant in the boundary layer.

layer and tested it with observations made at O'Neill, Nebr. Using the curve of Estoque's figure 12, we found by harmonic analysis the semidiurnal variation of the surface stress, $0.93 \sin(2\omega t + 51^\circ)$ dynes cm^{-2} . Then using the ratio of the coefficients in figure 4 at latitude 40° to estimate the components, we found $\delta\tau_\phi(0) = 0.63 \sin(2\omega t + 4^\circ)$ and $\delta\tau_\theta(0) = 0.68 \sin(2\omega t + 94^\circ)$ dynes cm^{-2} . If $\beta = 138^\circ + 180^\circ = 238^\circ$, the angle D is 26° and the implied value of h is nearly 24 km. However, over the Great Plains the low-level jet attains quite high speeds, and the semidiurnal motions and pressure forces may easily result in values several times larger than the values of the coefficients in equations (8) and (9). The equations are therefore not applicable to the unusual conditions during a low-level jet situation, and the actual depth of the boundary layer could be an order of magnitude smaller.

The depth h is not strictly the total depth of the layer of frictional influence, but the height above the lower boundary at which the frictional component of the wind becomes parallel to the wind induced by pressure forces. Ideally, one should be able to use the observed winds in table 3 to estimate the depth, as well as the angle D . In figure 6, the phase angles of v and u for the five low-latitude stations are plotted as functions of height. When friction is absent, according to the model of the progressive semidiurnal wave, the phase angle of v should be equal to the phase angle of the height variation (table 3, Appendix B) plus 180° . The phase angle of $-u$, the poleward component of the wind, should be equal to the

phase angle of the height variation minus 90°. However, the phase angles in figure 6, together with the tabulated height variations, show that this condition is never quite met, even in the upper troposphere. Three possible explanations for this disagreement in phase can be suggested: (1) friction is effective throughout the troposphere; (2) the pressures are in error as a result of the radiation error of the instrument; and (3) the basic model assumption, that the phase of S_2^2 is constant with colatitude, may be wrong. Of these possibilities, the last two seem most likely, the second becoming important, however, only above a height of several kilometers.

Since there is no means of verifying or correcting for either of these possible errors, h cannot be determined with any certitude. One approach to determining h would seem to be to choose the height at which the variation of wind with height becomes constant. Another approach, and the one implicit in the model of the semi-diurnal motions in the friction layer, is to choose the level at which the wind components attain the phase, indicated by the vertical lines in figure 6, appropriate to the surface pressure variation—which in the model is assumed to be independent of height. Both of these approaches yield a value of h of about 6 km. The value of D appears to be about 30°. When h and D have these values, and are independent of colatitude, the components of the surface stress are indicated by the curves in figure 4, the appropriate scale being at the right. We shall accept these curves as the best approximation to the surface stress that we can obtain from the observational data. The values are much smaller than those derived as residual quantities in the equations of motion. However, a still troubling feature is that a depth of 6 km. is much greater than that normally assumed as the depth of the planetary boundary layer. The result can perhaps be explained by the simplifying assumptions in the friction model, notably the neglect of the variations of K_m with time and height. Although the indicated values of the surface stress might be realistic, the implied depth of the friction layer could be a fictitious result of these restrictions. Additional observations on the behavior of the daily variation of the wind in the friction layer, and further analyses along the lines suggested by Estoque [3] should result in more reliable estimates of the semi-diurnal component of the surface stress.

5. NUMERICAL RESULTS

To compute the surface pressure variation $S_{2,2}^2(p)$ resulting from the variation of the surface stress, $\delta\tau_\phi(0)$ in equation (8) may be substituted into equation (2), yielding

$$S_{2,2}^2(p)_\tau = \frac{4\rho_0\omega M_2 V_p^2 \sin^3 \theta h \sin D}{h_2(V_p + U_p \cos \theta)(3\pi + 4D)} \cos(2\omega t + \beta + D). \quad (11)$$

The use of a function of $\delta\tau_\theta(0)$ instead of $\delta\tau_\phi(0)$ would not significantly alter the results. For the numerical

TABLE 2.—Amplitude (A , mb.) and phase (α , deg.) of thermal and frictional contributions to $S_{2,2}^2$, the observed semi-diurnal pressure variation, and the error of the computed values.

Station	Computed Pressure Variation						Observed minus Gravitational tide		Error	
	Thermal		Frictional		Total		A	α	A	α
	A	α	A	α	A	α				
Valparaiso.....	0.88	204	0.37	98	0.85	179	0.52	151	0.48	215
Bermuda.....	0.67	217	0.35	98	0.72	192	0.60	154	0.49	256
Fort Worth.....	1.91	177	0.33	98	2.00	167	0.84	154	1.20	178
Osan.....	0.78	231	0.29	98	0.63	149	0.52	149	0.11	149
Azores.....	1.00	207	0.25	98	0.95	192	0.51	158	0.62	222
Sault Ste. Marie.....	0.90	233	0.16	98	0.71	225	0.32	189	0.59	245
Stephenville.....	0.84	254	0.14	98	0.57	229	0.25	194	0.41	252
Keflavik.....	0.21	189	-----	-----	-----	-----	0.16	158	0.12	237
Thule.....	0.25	185	-----	-----	-----	-----	0.16	197	0.09	178

calculations we have used the values $T_0(0)=288^\circ\text{K.}$ and $T_0(\infty)=160^\circ\text{K.}$ adopted by Siebert. The resonance magnification, with $h_2=7.85$ km. is then 3.7.

The integral in equation (2) was evaluated numerically, with the values of δT_a inserted for each of the nine stations, for the layer between the surface and 25 mb. The computed surface pressure variation resulting from thermal forcing is shown in table 2. The contribution of the surface stress, with h as 6 km. and D as 30°, is also tabulated. The total contribution from thermal and frictional effects is compared with the observed pressure variation by computing the error.

Since, at Keflavik and Thule, friction according to the model would make a negligible contribution to the pressure wave, only the thermal contribution is tabulated. The standing wave is of considerable importance at these stations; hence the difference between the observed and computed pressure variations is not readily interpreted.

At the remaining stations, however, there is a suggestion of a correlation between the error in the computed variation and the thermal contribution. This correlation suggests that the computed thermal contribution is too large. It seems reasonable to explain the large magnitude of the temperature variation, and its early phase, as the combined effect of random errors in the data and the temperature bias in the observations. The latter could be expected to produce a fictitious contribution directed approximately toward 0600, or 270°.

6. DISCUSSION OF RESULTS

An interpretation of the results of the study is necessarily uncertain. A basis for evaluation appears to be the assumption that the model itself is fundamentally realistic. Siebert's model gave excellent results when he applied it to the lunar tide, in which the forcing function is known exactly. His introduction of the thermal forcing function into the equations is straightforward.

In order to eliminate as many errors as possible, we decided to combine the temperature data for the four

low-latitude stations which appear to be relatively homogeneous: Valparaiso, Bermuda, Osan, and the Azores. The data for Fort Worth, compared with that for the other stations, are anomalous in several respects, and it did not seem desirable to include inhomogeneous data in the final analysis of the results. Since the standing wave becomes important at Keflavik and Thule, and since the phase of the semidiurnal pressure variation at Sault Ste. Marie and Stephenville is also markedly different from that of the migrating wave, these stations were excluded from the averages.

The average diabatic temperature change at the four stations is plotted as a hodograph in figure 7. The layer in which eddy heat transfer appears to account for the temperature variation was estimated by determining the end point of the logarithmic spiral which is the characteristic signature of the transfer process. This spiral is plotted as the dashed curve on the diagram. The coefficient of turbulent heat transfer, K_h , assumed constant in the layer and in time, was found to be $2.98 \times 10^5 \text{ cm.}^2 \text{ sec.}^{-1}$.

It seems reasonable to assume that both sources of temperature error, random and systematic, are at a minimum in this layer where the temperature variation is largely controlled by transfer from the surface. The contribution of eddy transfer of heat to the surface pressure oscillation is readily found by substituting the smoothed values obtained from figure 7 into equation (2) and evaluating the integral.

Consideration of all the possible sources of error suggests that this computation, showing the effect of eddy heat transfer on the pressure oscillation, is probably the most accurate of the indications given by our analysis of the observations. Next in order of accuracy, we believe, is the contribution of friction, based on the friction model and on the indications of the wind observations. The latter, at least, contain no known systematic error. Insofar as the phase of the frictional contribution is concerned, there is little ambiguity, since the surface stress should be in the direction of the surface wind. However, the magnitude of the frictional component is subject to the uncertainties we have discussed, arising primarily from the assumption of constant K_m . Least reliable is the computation based on the temperature variation in the total layer, surface to 25 mb., with its high probability of appreciable random and systematic errors.

The results of the study, viewed in this light, are summarized in the harmonic dial of figure 8. The vector OP represents the observed pressure oscillation, about 1.2 mb. at the equator, after the gravitational tide according to Siebert's computation has been removed. The vectors based on the average thermal and frictional effects at the four stations were increased by the factor $1/\sin^3\theta$ in order to make them comparable with OP. The vector FP represents the contribution of surface friction with angle D taken as 30° and h as 6 km. Vector OT indicates the

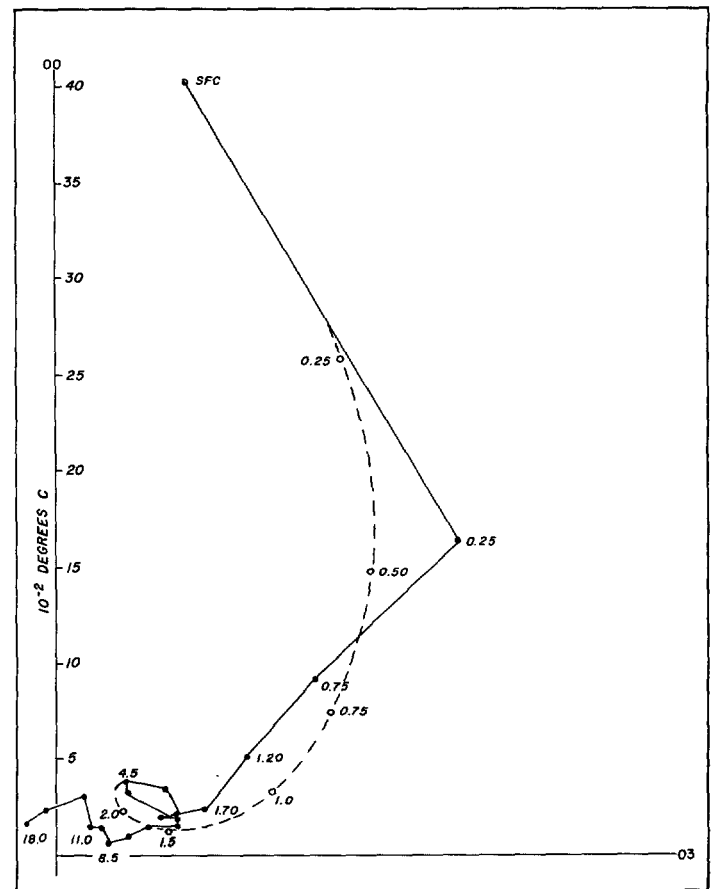


FIGURE 7.—Polar representation of the average diabatic temperature variation at the four stations Valparaiso, Bermuda, Osan, and the Azores. The logarithmic spiral representing the assumed temperature variation due to turbulent heat transfer from the surface is shown by the dashed curve. Heights on the observed and empirical hodographs are indicated in km. The amplitude of the variation is indicated by the temperature scale on the ordinate, and the phase is shown in hours.

phase and amplitude resulting from integration of the observed temperature variation throughout the layer for which data were available. Vector OE is the thermal contribution from eddy heat transfer alone. At the end of vector OE, we have added a vector EA, which Siebert concluded to be the thermal contribution resulting from the absorption of energy by water vapor and ozone.

As an aid in evaluating the results, lines x and y marking the theoretical limits of the phase of the frictional component are drawn on the diagram. These limits are determined by the permissible phases of the surface stress which, according to the friction model (equation (100), Appendix C), can vary up to a maximum of one and one-half hours before the time of the pressure-dependent wind. Dashed curves, labeled in km. indicate the depth of the friction layer corresponding to the phase and amplitude of the frictional component of the pressure variation. These curves approach the line x , asymptotically, at point P.

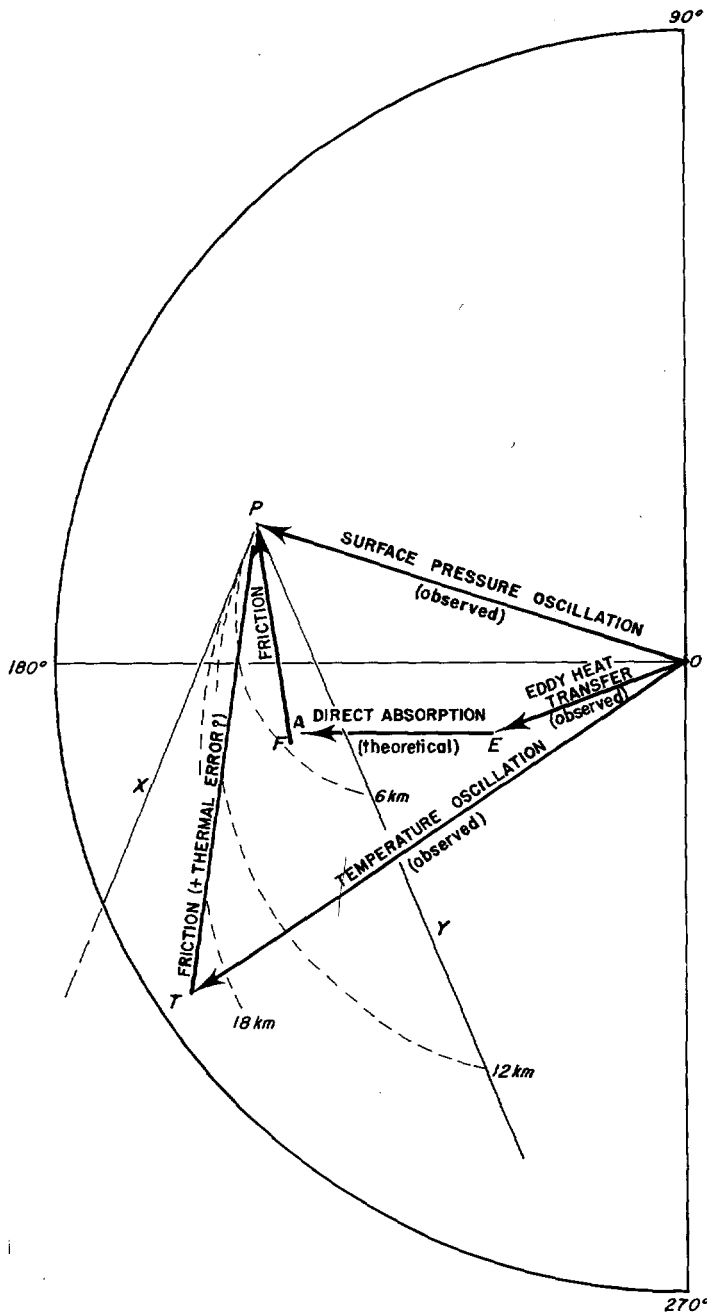


FIGURE 8.—Computed thermal and frictional components of the migrating semidiurnal pressure wave, S_2^2 . The lines x and y mark the theoretical limits of the phase of the frictional component. The dashed curves indicate the depth of the friction layer, in km, implied by the amplitude and phase of the frictional component.

If we take the computation represented by OT at face value, and assume that friction must account for the difference between OT and OP, the friction layer must be assumed to extend high into the stratosphere—subject of course to the uncertainties of the friction model. This consideration, combined with the known bias in the observed temperatures, suggests that OT should not be re-

garded as a reliable estimate of the thermally induced oscillation. The vectors OE, EA, and FP, when combined, very nearly give the magnitude and phase of the observed pressure wave. These vectors, OE, EA, and FP, were independently derived. The additional fact that they are based on theory as well as on observational data leads one to conclude that they offer a reasonable explanation for the semidiurnal pressure oscillation.

7. SUMMARY AND CONCLUSIONS

This study has attempted to determine, on the basis of theory and observations, the thermal and frictional contributions to the progressive part of the semidiurnal pressure wave. Friction was introduced into the equations of motion as a potential force, and the tidal equations were re-derived with the additional terms. The model atmosphere and boundary conditions adopted by Siebert served as a basis for numerical computations using the observational results from nine rawinsonde stations.

The upper-air data, extending from the surface to about 25 km., were analyzed to obtain the semidiurnal variations of pressure, temperature, and wind. The evaluation of the frictional forcing term is based on an extension, to the semidiurnal motions, of the Ekman theory of the boundary layer, assuming the coefficient of eddy exchange of momentum to be constant. The observed winds and their variation with height indicate the values of the parameters, depth of friction layer, and angle of surface flow, necessary to compute the surface stress. An empirical estimate of the mean semidiurnal wind components offers a first approximation to the distribution of friction with colatitude, and suggests that the assumption of friction as a potential force is valid for the semidiurnal tide.

The conclusions are tentative, since there are a number of possible sources of error in the numerical results: some too-restrictive assumptions in the model, and systematic as well as random errors in the observational data. The probable existence of a bias in the observed temperatures, large in the stratosphere and perhaps extending downward into the troposphere, makes the results of the thermal computation doubtful. The temperature errors are believed to be small or negligible in the lower troposphere. Here, the diabatic temperature variation is closely described by a logarithmic spiral and is assumed to be controlled by eddy transfer of heat from the surface. This computation appears to be the most reliable of the several made, and indicates that eddy transfer of heat is a significant tide-producing force.

The computation of the frictional component of the wave must be regarded as approximate only, for a large value of the depth of the planetary boundary layer must be assumed. This depth, however, may be a fictitious result of the simplifications inherent in the friction model. There is thus a good possibility that the frictional contribution to the tide has not been overestimated. Support

for this view comes from the fact that the contributions to the wave from eddy transfer of heat and momentum, added to that derived by Siebert as the effect of direct absorption of heat by water vapor and ozone, nearly explain the observed pressure oscillation. However, the results must be considered tentative, particularly in view of the known variations of K_m with height and time.

The results, though preliminary, suggest that the necessity for a larger contribution to the tide by ozone heating is open to question. Further observational studies of the semidiurnal variation of surface stress, and of the semidiurnal temperature variation in the turbulent boundary layer, appear to offer promising avenues for refining our knowledge of the physical processes resulting in the tidal oscillation.

APPENDIX A

In the theory of atmospheric tides, the earth is assumed to be a sphere of radius a and to rotate with uniform angular velocity ω . The change of acceleration of gravity g with colatitude and height is neglected. Vertical accelerations and horizontal advective terms in the equations can also be neglected in view of the large horizontal scale of the oscillations. The tidal variations are thus regarded as small perturbations superimposed on an undisturbed atmosphere in which the static pressure p_0 , density ρ_0 , and temperature T_0 depend on height z but not on colatitude θ or longitude ϕ . The hydrostatic equation for the undisturbed atmosphere is thus

$$\frac{dp_0}{dz} = -g\rho_0 \quad (12)$$

and the equation of state is

$$p_0 = R\rho_0 T_0 = g\rho_0 H \quad (13)$$

in which R is the universal gas constant for (dry) air and H is the scale height

$$H = \frac{RT_0}{g} \quad (14)$$

To these basic assumptions we add the condition that the perturbation value of the vertical flux of momentum, $\partial\delta\tau/\partial z$, be represented as a potential force, so that we can use the approximation

$$-\frac{1}{a} \frac{\partial}{\partial\theta} \left(\frac{\partial\delta\tau}{\partial z} \right) \approx \frac{\partial\delta\tau_\theta}{\partial z} \quad (15)$$

$$-\frac{1}{a \sin\theta} \frac{\partial}{\partial\phi} \left(\frac{\partial\delta\tau}{\partial z} \right) \approx \frac{\partial\delta\tau_\phi}{\partial z} \quad (16)$$

Since the perturbation pressure and density are defined by

$$p = p_0 + \delta p, \text{ and } \rho = \rho_0 + \delta\rho \quad (17)$$

the equations of motion in spherical polar coordinates may be written

$$\frac{\partial u}{\partial t} - 2\omega v \cos\theta = -\frac{1}{a} \frac{\partial}{\partial\theta} \left(\frac{\delta p}{\rho_0} + \Omega + \frac{1}{\rho_0} \frac{\partial\delta\tau}{\partial z} \right) \quad (18)$$

$$\frac{\partial v}{\partial t} + 2\omega u \cos\theta = -\frac{1}{a \sin\theta} \frac{\partial}{\partial\phi} \left(\frac{\delta p}{\rho_0} + \Omega + \frac{1}{\rho_0} \frac{\partial\delta\tau}{\partial z} \right) \quad (19)$$

$$\frac{\partial\delta p}{\partial z} = -g\delta\rho - \rho_0 \frac{\partial\Omega}{\partial z} \quad (20)$$

where u is the equatorward, v the eastward component of the perturbation velocity, and Ω is the tidal potential. To these equations must be added the equation of continuity

$$\frac{D\rho}{Dt} + \rho_0 \chi = 0 \quad (21)$$

where

$$\text{div } \mathbf{V} = \chi = \frac{1}{a \sin\theta} \frac{\partial}{\partial\theta} (u \sin\theta) + \frac{1}{a \sin\theta} \frac{\partial v}{\partial\phi} + \frac{\partial w}{\partial z} \quad (22)$$

w being the vertical component of the perturbation velocity; and the first law of thermodynamics for an ideal gas

$$\delta Q = c_v dT + p d \left(\frac{1}{\rho} \right) \quad (23)$$

If δQ is proportional to dT the changes of state occur polytropically and are given by

$$\delta Q = \Gamma dT; T \propto p^{\gamma-1} \quad (24)$$

where

$$\gamma = \frac{c_p + \Gamma}{c_v + \Gamma}, \quad 0 \leq \Gamma < \infty.$$

When $\Gamma = 0$, equation (24) becomes the equation for adiabatic changes of state

$$\delta Q = 0; T \propto \rho^{\gamma-1} \quad (25)$$

and

$$\gamma = \frac{c_p}{c_v} = 1.40.$$

If $\delta Q = 0$, the only temperature variation is that caused by adiabatic changes of state and is defined by Siebert as a *secondary* temperature variation. A *primary* (diabatic) temperature variation, produced by influences outside the atmosphere, may be described by

$$\delta Q = J dT. \quad (26)$$

Using (26) to eliminate δQ in (23), and introducing γ from (25) by use of the equation

$$R = c_p - c_v \quad (27)$$

we obtain

$$\frac{R}{\gamma-1} \frac{DT}{Dt} = \frac{p}{\rho^2} \frac{D\rho}{Dt} + J \quad (28)$$

and, with the aid of the gas equation (13)

$$\frac{dp}{p} = \frac{d\rho}{\rho} + \frac{dT}{T} \quad (29)$$

With (14) and (17), two equivalent forms of the first law of thermodynamics are obtained; neglecting small quantities,

$$\frac{R}{\gamma-1} \frac{DT}{Dt} = \frac{gH}{\rho_0} \frac{D\rho}{Dt} + J \tag{30}$$

and

$$\frac{Dp}{Dt} = \gamma gH \frac{D\rho}{Dt} + (\gamma-1)\rho_0 J \tag{31}$$

where the individual operator reduces to

$$\frac{Dp}{Dt} = w \frac{dp_0}{dz} + \frac{\partial \delta p}{\partial t} \tag{32}$$

With these basic physical equations, we can derive solutions for the pressure and temperature variations and the velocity components associated with the tidal oscillations. Because only periodic variations are considered, we can put

$$u, v, w, \delta p, \delta \rho, \delta T, \chi, \Omega, J, \frac{\partial \delta \tau}{\partial z} \propto e^{i\sigma t} \tag{33}$$

where σ is the angular frequency of the oscillation. Introducing (33), we solve equations (18) and (19) for u and v :

$$u = \frac{\sigma}{4a\omega^2(f^2 - \cos^2 \theta)} \left[i \frac{\partial}{\partial \theta} + \frac{\cot \theta}{f} \frac{\partial}{\partial \phi} \right] \left(\frac{\delta p}{\rho_0} + \Omega + \frac{1}{\rho_0} \frac{\partial \delta \tau}{\partial z} \right) \tag{34}$$

$$v = \frac{i\sigma}{4a\omega^2(f^2 - \cos^2 \theta)} \left[i \frac{\cos \theta}{f} \frac{\partial}{\partial \theta} + \frac{1}{\sin \theta} \frac{\partial}{\partial \phi} \right] \left(\frac{\delta p}{\rho_0} + \Omega + \frac{1}{\rho_0} \frac{\partial \delta \tau}{\partial z} \right) \tag{35}$$

in which

$$f = \frac{\sigma}{2\omega} \tag{36}$$

We now substitute u and v from equations (34) and (35) into equation (22), obtaining

$$\chi = \frac{\partial w}{\partial z} + \frac{i\sigma}{4a^2\omega^2} F \left(\frac{\delta p}{\rho_0} + \Omega + \frac{1}{\rho_0} \frac{\partial \delta \tau}{\partial z} \right) \tag{37}$$

in which F is the differential operator

$$F = \frac{1}{\sin \theta} \frac{\partial}{\partial \theta} \left(\frac{\sin \theta}{f^2 - \cos^2 \theta} \frac{\partial}{\partial \theta} \right) + \frac{1}{f^2 - \cos^2 \theta} \left(\frac{i}{f} \frac{f^2 + \cos^2 \theta}{f^2 - \cos^2 \theta} \frac{\partial}{\partial \phi} + \frac{1}{\sin^2 \theta} \frac{\partial^2}{\partial \phi^2} \right) \tag{38}$$

By following Siebert's development closely from this point, we derive the equations for a model identical in every respect with Siebert's except for the appearance of terms involving friction. Substituting the equation of continuity into (30), and using (14) and (33), we find

$$i\sigma \delta T = \frac{\kappa}{R} \left(\gamma J - \gamma g H \chi - \frac{wg}{\kappa} \frac{dH}{dz} \right) \tag{39}$$

where

$$\kappa = \frac{\gamma-1}{\gamma} = \frac{c_p - c_v}{c_p} = \frac{2}{7} \tag{40}$$

Then with equations (21), (31), (12), and expression (33) we have

$$i\sigma \delta p = wg\rho_0 - \gamma g\rho_0 H \chi + (\gamma-1)\rho_0 J. \tag{41}$$

When (41) and (13) are differentiated with respect to z , and (12) is introduced, δp and $\delta \rho$ may be eliminated. Then with the aid of (20) and (21), we find

$$\frac{\partial w}{\partial z} = \gamma H \frac{\partial \chi}{\partial z} - (\gamma-1)\chi - \frac{\gamma-1}{g\rho_0} \frac{\partial}{\partial z} (\rho_0 J) - \frac{i\sigma}{g} \frac{\partial \Omega}{\partial z}. \tag{42}$$

Differentiating equations (37) and (42) with respect to z , we eliminate $\partial^2 w / \partial z^2$ between the resulting equations, neglecting a term $\partial^2 \Omega / \partial z^2$ which is small in comparison with $\partial \Omega / \partial z$. Then differentiating $\delta p / \rho_0$ [eqn. (30)] with respect to z , we eliminate $\partial w / \partial z$ by means of (42) and combine (12) and (13) to obtain

$$\frac{1}{\rho_0} \frac{d\rho_0}{dz} = -\frac{1}{H} \left(1 + \frac{dH}{dz} \right). \tag{43}$$

We can now use these relations to derive a partial differential equation for χ :

$$H \frac{\partial \chi}{\partial z} + \left(\frac{dH}{dz} - 1 \right) \frac{\partial \chi}{\partial z} - \frac{\kappa}{g} \frac{\partial}{\partial z} \left[\frac{\partial J}{\partial z} - \left(1 + \frac{dH}{dz} \right) \frac{J}{H} \right] - \frac{g}{4a^2\omega^2} F \left\{ \left(\kappa + \frac{dH}{dz} \right) \chi - \frac{\kappa}{gH} \left(1 + \frac{dH}{dz} \right) J - \frac{i\sigma}{\gamma g \rho_0} \left[\frac{\partial^2 \delta \tau}{\partial z^2} + \frac{1}{H} \left(1 + \frac{dH}{dz} \right) \frac{\partial \delta \tau}{\partial z} \right] \right\} = 0. \tag{44}$$

Equation (44) may be solved by the method of separation of variables, after representing χ , J , and $\partial \delta \tau / \partial z$ by series expansions in terms of the eigenfunctions $\psi_n(\theta, \phi)$ of the operator F :

$$\begin{aligned} \chi &= \sum_n \chi_n(z) \psi_n(\theta, \phi) e^{i\sigma t} \\ J &= \sum_n J_n(z) \psi_n(\theta, \phi) e^{i\sigma t} \\ \frac{\partial \delta \tau}{\partial z} &= \sum_n \left(\frac{\partial \delta \tau}{\partial z} \right)_n(z) \psi_n(\theta, \phi) e^{i\sigma t}. \end{aligned} \tag{45}$$

Substituting χ , J , and $\partial \delta \tau / \partial z$ from these expressions into (44) and denoting the constant of separation by $1/h_n$, we obtain the ordinary differential equations

$$F\psi_n + \frac{4a^2\omega^2}{g h_n} \psi_n = 0 \tag{46}$$

$$\begin{aligned}
 H \frac{d^2 \chi_n}{dz^2} + \left(\frac{dH}{dz} - 1 \right) \frac{d\chi_n}{dz} + \left(\kappa + \frac{dH}{dz} \right) \frac{\chi_n}{h_n} \\
 = \frac{\kappa}{g} \left\{ \left(1 + \frac{dH}{dz} \right) \frac{J_n}{H h_n} - \frac{d}{dz} \left[\left(1 + \frac{dH}{dz} \right) \frac{J_n}{H} \right] + \frac{d^2 J_n}{dz^2} \right\} \\
 + \frac{i\sigma}{\gamma g \rho_0 h_n} \left[\frac{d^2 \delta \tau_n}{dz^2} + \left(1 + \frac{dH}{dz} \right) \frac{1}{H} \frac{d\delta \tau_n}{dz} \right]. \quad (47)
 \end{aligned}$$

Now if we assume that $u, v, w, \delta p, \delta T$, and Ω can also be represented by series expansions corresponding to (45) it follows from (37), (42), (43), and (46) that

$$\frac{\delta p_n}{\rho_0} + \Omega_n + \frac{1}{\rho_0} \frac{d\delta \tau_n}{dz} = \frac{\gamma g h_n}{i\sigma} \left[\left(H \frac{d}{dz} - 1 \right) \left(\chi_n - \frac{\kappa}{g} \frac{J_n}{H} \right) \right] \quad (48)$$

in which a term $h_n d\Omega_n/dz$ has been neglected in comparison with Ω_n . Then expanding δp in (41) and substituting δp_n for w_n in (48), we find

$$\begin{aligned}
 w_n = -\frac{i\sigma}{g} \Omega_n + \gamma \left[\left(H h_n \frac{d}{dz} + H - h_n \right) \right. \\
 \left. \left(\chi_n - \frac{\kappa J_n}{g H} \right) \right] - \frac{i\sigma}{g p_0} \frac{d\delta \tau_n}{dz}. \quad (49)
 \end{aligned}$$

With these results, u_n, v_n , and δT_n in (34), (35), and (39) can be expressed as functions of χ_n, Ω_n, J_n , and $\delta \tau_n$ and their derivatives. However, a simplification is possible by the following transformation of variables:

$$x = \int_0^z \frac{d\xi}{H(\xi)} \quad (50)$$

$$y_n(x) e^{x/2} = \chi_n(z) - \frac{\kappa J_n(z)}{g H(z)} - \frac{i\sigma \delta \tau_n(z)}{\gamma g h_n \rho_0(z) H(z)}. \quad (51)$$

With equation (50), the distribution of static pressure becomes

$$p_0(x) = p_0(0) e^{-x} \quad (52)$$

and with (50) and (51) the differential equation (47) may be transformed to obtain

$$\begin{aligned}
 \frac{d^2 y_n}{dx^2} - \frac{1}{4} \left[1 - \frac{4}{h_n} \left(\kappa H(x) + \frac{dH}{dx} \right) \right] y_n(x) = \frac{\kappa J_n(x)}{\gamma g h_n} e^{-x/2} \\
 + \frac{i\sigma}{\gamma g \rho_0(x) h_n^2} \left(1 + \frac{1}{H} \frac{dH}{dx} \right) \delta \tau_n(x) e^{-x/2}. \quad (53)
 \end{aligned}$$

The same transformation can be applied to equations (48) and (49), after elimination of ρ_0 by means of (13), and to equations (34), (35), and (39). Then the coefficients of the series expansions are given by the following equations:

$$\begin{aligned}
 u_n(x) = \frac{\gamma g h_n e^{x/2}}{4a\omega^2(f^2 - \cos^2 \theta)} \left(\frac{dy_n}{dx} - \frac{1}{2} y_n \right) \\
 + \frac{i\sigma e^{-x/2}}{\gamma g h_n \rho_0(x) H(x)} \frac{d\delta \tau_n}{dx} \left(\frac{\partial}{\partial \theta} - \frac{i \cot \theta}{f} \frac{\partial}{\partial \phi} \right) \quad (54)
 \end{aligned}$$

$$\begin{aligned}
 v_n(x) = \frac{i\gamma g h_n e^{x/2}}{4a\omega^2(f^2 - \cos^2 \theta)} \left(\frac{dy_n}{dx} - \frac{1}{2} y_n \right) \\
 + \frac{i\sigma e^{-x/2}}{\gamma g h_n \rho_0(x) H(x)} \frac{d\delta \tau_n}{dx} \left(\frac{\cos \theta}{f} \frac{\partial}{\partial \theta} - \frac{i}{\sin \theta} \frac{\partial}{\partial \phi} \right) \quad (55)
 \end{aligned}$$

$$\begin{aligned}
 w_n(x) = -\frac{i\sigma}{g} \Omega(x) + \gamma h_n e^{x/2} \left[\frac{dy_n}{dx} + \left(\frac{H(x)}{h_n} - \frac{1}{2} \right) y_n \right] \\
 + \frac{i\sigma}{g h_n \rho_0(x)} \delta \tau_n(x) \quad (56)
 \end{aligned}$$

$$\delta p_n(x) = \frac{p_0(0)}{H(x)} \left[-\frac{\Omega_n(x)}{g} e^{-x} + \frac{\gamma h_n}{i\sigma} e^{-x/2} \left(\frac{dy_n}{dx} - \frac{1}{2} y_n \right) \right] \quad (57)$$

$$\begin{aligned}
 \delta T_n(x) = \frac{1}{R} \left\{ \frac{\Omega_n(x)}{H(x)} \frac{dH}{dx} - \frac{\gamma g h_n}{i\sigma} e^{x/2} \left[\frac{\kappa H(x)}{h_n} + \frac{1}{H(x)} \frac{dH}{dx} \right. \right. \\
 \left. \left. \left(\frac{d}{dx} + \frac{H(x)}{h_n} - \frac{1}{2} \right) y_n \right] + \frac{1}{R} \left\{ \frac{\kappa J_n(x)}{i\sigma} + \frac{g}{p_0(0)} e^x \right. \right. \\
 \left. \left. \left[\left(\frac{\kappa H(x)}{h_n} - \frac{1}{h_n} \frac{dH}{dx} \right) \delta \tau_n(x) - \frac{1}{H(x)} \frac{dH}{dx} \frac{d\delta \tau_n}{dx} \right] \right\} \right\}. \quad (58)
 \end{aligned}$$

With the usual boundary condition that the vertical component of the velocity vanish at the earth's surface, equation (56) becomes

$$\left[\frac{dy_n}{dx} + \left(\frac{H}{h_n} - \frac{1}{2} \right) y_n \right]_{x=0} = \frac{i\sigma}{\gamma h_n} \left[\frac{\Omega_n(0)}{g} - \frac{H(0)}{h_n p_0(0)} \delta \tau_n(0) \right]. \quad (59)$$

For a second boundary condition, Siebert makes the reasonable assumption that the kinetic energy per column of unit cross-section must be finite

$$\int_0^\infty \rho_0(x) \mathbf{V}^2(x) H(x) dx < \infty. \quad (60)$$

Then when ρ_0 is eliminated by means of (12) and (50) and (52), \mathbf{V} replaced by its components (54), (55), and (56), and H assumed to remain finite for $x \rightarrow \infty$, we find from (60) that as $x \rightarrow \infty$, y_n must vanish more rapidly than $x^{-1/2}$:

$$y_n = 0(1/\sqrt{x}); \text{ or } \lim_{x \rightarrow \infty} [y_n(x) \cdot \sqrt{x}] = 0. \quad (61)$$

This boundary condition is not applicable to wave types with small h_n values if model atmospheres with isothermal tops are used. However, for the numerical computations limited to $S_{2,2}$, $h_n = h_2 = 7.85$ km., and the boundary condition may be used.

It follows from (57) and (59) that the surface pressure variation is given by

$$\delta p_n(0) = \frac{i\gamma}{\sigma} p_0(0) y_n - \frac{p_0(0)}{h_n} \delta \tau_n(0). \quad (62)$$

In the above development, equations (12) to (14) and (18) to (62) are either identical with or analogous to Siebert's equations (3.1) to (3.3) and (3.7) to (3.51), respectively, the only differences arising from the inclusion of the frictional terms in our development. Application of the theory requires the use of a model atmosphere, determined by the vertical distribution of the scale height, and the appropriate numerical values of the equivalent depth h_n . As the model atmosphere which most closely resembles the real atmosphere yet leads to elementary solutions, Siebert assumes

$$H(x) = \Delta H e^{-\kappa x} + H(\infty) \tag{63}$$

with

$$\Delta H = H(0) - H(\infty) \geq 0. \tag{64}$$

Replacing H in equations (53) and (63), Siebert obtains the equation

$$\frac{d^2 y_n}{dx^2} - \frac{1}{4} \left(1 - \frac{4\kappa H(\infty)}{\hat{h}_n} \right) y_n = 0. \tag{65}$$

Applying the boundary condition (61), he finds that only one of the two exponential functions satisfying (65) can be used:

$$y_n(x) = A_n \exp \left[-\frac{x}{2} \left(1 - \frac{4\kappa H(\infty)}{\hat{h}_n} \right)^{1/2} \right] \tag{66}$$

where A_n is an arbitrary constant. When h_n is substituted for \hat{h}_n , and equation (66) for $y_n(0)$ is substituted into (59), we can determine the integration constant A_n :

$$A_n = \frac{2i\sigma}{\gamma g} \cdot \frac{\Omega_n(0) - \frac{gH(0)}{h_n p_0(0)} \delta\tau_n(0)}{2H(0) - h_n(1 + \beta_n)} \tag{67}$$

where

$$\beta_n = + \sqrt{1 - 4\kappa \frac{H(\infty)}{h_n}}. \tag{68}$$

With the known A_n we now substitute $y_n(0)$ from (55) into (62), introducing the equilibrium tide $\overline{\delta p_n} = -\rho_0 \Omega_n$ and using equation (13) to obtain

$$\delta p_n(0) = \frac{2H(0)}{2H(0) - h_n(1 + \beta_n)} \left[\overline{\delta p_n(0)} + \frac{\delta\tau_n(0)}{h_n} \right]. \tag{69}$$

The determination of the equivalent depth h_n appropriate to each wave type by solution of equation (46) is described by Siebert. The appropriate h_n for $S_{2,2}^2$, the major component of the migrating semidiurnal tide, is 7.85 km., and the resonance magnification M_n , when we use the appropriate model (52) of the atmosphere, is

$$M_2 = \left| \frac{2H(0)}{2H(0) - h_n(1 + \beta_n)} \right|. \tag{70}$$

With the defining relation (5) between $\delta\tau_n$ and the latitudinal component of the stress, for a wave with $s=2$, we can rewrite equation (69) as

$$\delta p_n(0) = M_n \left[\overline{\delta p_n(0)} + \frac{a \sin \theta}{2h_n} i \delta\tau_{\phi,n}(0) \right]. \tag{71}$$

Thus, for known values of the equilibrium tide and observed values of the surface stress one can compute the resulting variation in surface pressure for wave type $S_{2,2}^2$, when appropriate values of $H(0)$ and $H(\infty)$ are used.

Since Siebert's derivation of the thermal tide is thoroughly covered in his survey, we shall simply quote his results here for the contribution to the surface pressure oscillation of the diabatic temperature variation δT_d in the layer bounded by x_1 and x_2 :

$$\delta p_n(0) = -\frac{p_0(0)}{T_0(0)} M_n \int_{x_1}^{x_2} \delta T_{d,n}(x) y_n^0(x) e^{-x/2} dx \tag{72}$$

with

$$y_n^0(x) = e^{-\beta_n x/2}, \quad h_n \geq 4\kappa H(\infty). \tag{73}$$

Thus the total contribution to the surface pressure variation for this wave type is given by

$$S_{2,2}^2(p) = M_2 \left[\overline{\delta p_2(0)} + \frac{a \sin \theta}{2h_2} i \delta\tau_{\phi,2}(0) - \frac{p_0(0)}{T_0(0)} \int_{x_1}^{x_2} \delta T_{d,2}(x) y_2^0(x) e^{-x/2} dx \right]. \tag{74}$$

APPENDIX B

The observed diurnal and semidiurnal variations of temperature, wind, and height of isobaric surfaces are tabulated in table 3 (pages 440-444). Estimates of the height variations computed from the observed wind variations are presented in table 4 (page 445).

(Appendix C follows on page 444.)

TABLE 3.—Amplitude (A), phase (α), and probable error (ϵ) of the observed diurnal (Parts A-1 through A-9) and semidiurnal (Parts B-1 through B-9) variations in temperature, isobaric height, and northward and eastward wind components at nine rawinsonde stations, for period July 1956 to June 1958. Phase: degrees. Amplitude and probable error: for surface pressure, mb.; height, 10⁻¹ m.; temperature, 10⁻² °C.; wind, cm. sec.⁻¹.

Height				Temperature			Northward Wind Component			Eastward Wind Component		
p_0	A	α	ϵ	A	α	ϵ	A	α	ϵ	A	α	ϵ
Part A-1—Eglin Air Force Base, Valparaiso, Fla. (30°29' N., 86°31' W.)												
SFC	0.59	325	0.05	319	242	14	44	241	6	51	229	5
1000	52	313	4	168	227	12	6	261	4	41	260	5
950	38	301	4	71	202	8	44	58	5	53	300	4
900	52	285	4	37	185	5	73	62	8	69	314	5
850	51	280	4	22	165	4						
800	49	276	4	17	147	4	73	65	9	72	316	5
750	51	274	7	13	157	4	56	70	9	62	316	6
700	46	269	5	16	148	3	38	76	6	46	313	5
650	41	265	5	17	161	4	24	85	5	29	309	6
600	46	261	5	16	182	3	9	87	6	15	298	7
550	43	250	6	20	180	3	5	300	7	8	257	7
500	30	258	11	21	191	5	13	290	8	9	198	7
450	51	239	6	22	214	4	13	207	9	10	178	7
400	63	239	6	23	229	4	11	202	10	10	173	8
350	73	238	7	24	241	4	12	291	10	11	167	8
300	85	239	7	24	244	4	12	273	9	14	148	6
250	100	239	8	29	262	4	16	248	8	21	131	6
200	120	244	9	38	273	4	25	232	7	28	121	4
175	132	247	10	41	288	3	36	234	5	33	130	5
150	145	252	10	38	293	3	44	241	6	39	143	8
125	159	255	11	34	288	4	45	244	6	43	153	9
100	173	257	13	39	279	5	41	244	5	40	153	8
80	210	259	15	51	282	5	34	246	5	30	151	6
60	262	262	17	84	272	6	27	251	9	19	152	8
50	308	264	19	87	284	6	21	252	12	11	164	11
40	360	266	19	93	281	8	19	238	12	11	158	11
30	439	268	18	100	278	6	26	232	13	21	123	12
20	560	266	22	128	270	9	38	230	13	45	97	15
15	710	268	32	165	273	13	51	242	14	70	84	21
10	1086	275	50	230	275	5	87	224	40	139	71	98
Part A-2—St. George, Bermuda (32°22' N., 64°40' W., 17 ft.)												
SFC	0.18	279	0.03	59	257	4	9	109	3	11	287	3
1000	18	275	2	40	249	3	10	89	2	10	302	2
950	20	276	4	21	237	3	14	74	2	11	323	2
900	24	261	2	16	214	3	19	66	2	13	330	2
850	26	256	2	18	212	4						
800	27	252	2	15	224	3	20	58	2	14	327	2
750	29	259	3	15	219	3	19	49	3	16	318	3
700	32	246	2	14	209	2	16	42	3	20	311	3
650	37	242	4	17	222	2	13	42	2	25	302	3
600	38	241	2	15	241	3	11	22	2	28	296	3
550	41	239	5	13	260	3	14	346	3	28	288	4
500	46	240	3	14	250	3	21	317	3	20	277	5
450	57	241	7	17	245	3	26	296	3	12	244	6
400	57	242	5	18	252	2	29	272	4	10	171	7
350	64	241	5	18	242	3	33	255	6	16	128	9
300	72	240	6	22	247	3	42	245	9	27	106	10
250	85	240	7	24	247	3	51	247	9	41	96	10
200	100	242	7	24	282	5	56	256	9	50	95	10
175	105	246	8	26	298	4	59	271	8	51	98	10
150	113	249	8	22	292	5	59	287	8	41	100	10
125	119	251	11	21	285	5	50	298	7	32	97	8
100	136	253	11	38	272	4	34	296	8	34	93	6
80	160	255	11	52	270	4	23	264	8	46	99	4
60	197	254	13	53	271	5	30	236	8	53	109	6
50	229	255	14	65	269	5	36	236	8	45	124	9
40	283	257	15	90	268	6	36	247	8	32	151	10
30	357	257	19	103	275	7	36	259	8	30	173	10
20	510	260	27	138	268	11	40	263	10	36	162	11
15	603	263	34	149	273	14	42	267	12	52	145	14
10												
Part A-3—Ft. Worth, Tex. (32° 50' N., 97° 3' W., 576 ft.)												
SFC	1.07	343	0.08	431	225	25	59	92	14	87	344	18
1000	97	345	8	294	218	38	79	93	18	100	351	20
950	69	332	7	205	195	25	81	99	21	100	359	20
900	59	301	7	92	182	21	51	99	21	100	359	20
850	54	292	8	41	171	13	51	117	19	68	10	16
800	51	285	9	24	169	6	24	188	15	22	31	10
750	51	276	8	24	172	3	41	254	11	21	180	5
700	48	272	8	28	179	4	59	281	9	44	201	6
650	51	264	8	31	183	5	74	298	8	57	213	10
600	51	255	9	32	192	6	85	311	10	60	224	13
550	56	251	10	29	206	6	89	320	11	58	231	15
500	62	243	11	27	217	4	84	324	9	49	233	14
450	69	242	11	26	222	5	73	322	8	34	226	14
400	78	238	13	25	221	4	62	309	9	19	195	12
350	88	236	14	26	230	5	60	286	11	20	139	11
300	100	234	14	27	229	3	65	262	13	30	111	12
250	116	231	15	26	224	4	70	240	14	39	98	13
200	133	229	15	27	255	4	74	222	12	47	93	12
175	140	232	16	29	254	4	73	212	10	49	96	9
150	151	232	16	35	266	4	66	213	7	45	110	7
125	176	238	18	38	271	6	59	223	4	43	130	4
100	198	244	15	44	281	8	58	234	4	42	145	3
80	268	244	28	45	262	15	65	243	6	41	160	3
60	323	246	22	80	276	11	61	261	8	32	183	4
50	353	245	34	63	279	8	47	279	7	23	211	5
40	385	246	40	59	270	8	27	286	4	15	247	6
30	429	249	39	79	271	9	13	234	6	18	284	6
20	427	250	39	79	261	16	28	188	13	34	288	6
15												
10												
Part A-4—Osan, Korea (37°6' N., 127°2' E.)												
SFC	0.61	8	0.04	311	234	19	14	269	3	54	200	6
1000	43	1	4	216	227	20	15	246	4	40	186	6
950	27	355	4	94	204	7	16	210	4	24	157	5
900	22	308	4	46	188	4	17	172	3	11	105	3
850	20	293	4	28	188	4						
800	20	280	4	18	201	4	17	148	3	8	11	3
750	27	274	5	16	218	4	11	129	3	15	317	4
700	27	271	5	14	230	4	5	97	3	23	302	4
650	31	268	5	12	249	4	5	10	3	32	294	4
600	29	264	5	12	267	5	10	8	3	28	289	4
550	32	260	8	13	248	5	15	10	3	36	289	4
500	36	261	7	17	244	6	20	11	5	37	292	5
450	44	258	9	18	249	8	23	9	7	34	283	7
400	47	256	10	20	232	6	23	9	11	37	259	7
350	56	252	12	25								

Table 3.—Continued

SFC	Height			Temperature			Northward Wind Component			Eastward Wind Component			
	P_a	A	α	ϵ	A	α	ϵ	A	α	ϵ	A	α	ϵ
Part A-5.—Terceira, Azores (38°45' N., 27°5' W., 177 ft.)													
1000	0.11	149	0.04	112	259	9	11	328	4	2	268	3	
950	9	166	3	75	255	5	16	310	5	7	269	4	
900	11	173	5	27	244	3	21	298	6	5	264	5	
850	14	210	3	16	221	5	22	295	6	4	254	6	
800	17	209	3	18	206	5	18	295	7	2	189	5	
750	21	208	4	15	203	6	13	310	6	4	129	5	
700	23	208	4	18	220	4	10	331	6	3	123	5	
650	27	211	4	14	249	4	13	343	6	7	102	5	
600	31	217	5	13	237	4	13	344	6	3	127	5	
550	35	226	6	18	240	3	16	342	8	14	135	3	
500	40	222	6	18	241	4	16	337	8	16	124	3	
450	45	211	8	20	227	4	15	331	9	14	92	3	
400	57	222	7	19	241	5	13	313	9	9	41	4	
350	63	224	9	22	253	3	15	299	8	4	290	6	
300	75	229	9	23	255	6	24	288	7	21	210	7	
250	88	235	9	27	264	3	31	278	6	37	197	7	
200	105	238	9	29	263	4	35	267	6	39	189	7	
175	115	240	9	29	265	5	30	254	5	28	187	5	
150	128	242	10	39	278	3	22	235	4	17	182	4	
125	141	250	10	39	281	5	17	211	4	17	162	3	
100	169	253	9	43	275	3	20	204	3	24	145	3	
80	195	255	11	51	276	5	25	216	3	28	141	4	
60	230	258	11	65	272	4	28	233	4	25	141	5	
50	268	257	12	67	272	4	27	244	4	15	143	5	
40	310	257	13	73	266	4	27	252	5	13	175	4	
30	381	256	15	94	262	6	34	261	6	19	190	4	
20	501	256	22	132	264	7	48	268	7	26	177	7	
15	630	256	26	140	261	9	65	270	7	33	150	11	
10	852	256	63	197	259	23	73	266	7	47	125	15	

SFC	Height			Temperature			Northward Wind Component			Eastward Wind Component					
	p_0	A	α	ϵ	A	α	ϵ	A	α	ϵ	A	α	ϵ		
Part A-7.—Stephenville, Newfoundland (48°32' N., 58°33' W., 44 ft.)															
1000	0.14	94	0.06	152	247	17	152	247	17	23	314	4	71	241	7
950	8	118	5	131	244	16	131	244	16	23	309	4	51	243	6
900	9	184	5	52	220	10	52	220	10	22	297	4	27	252	4
850	14	204	4	15	184	7	15	184	7	17	285	4	13	275	4
800	18	203	4	14	221	6	14	221	6	8	278	5	10	287	5
750	23	216	4	17	226	4	17	226	4	3	44	7	7	272	6
700	23	209	5	16	239	4	13	239	4	13	75	6	3	262	7
650	21	217	7	21	225	5	22	225	5	22	78	5	3	50	6
600	31	216	5	22	231	5	22	231	5	28	80	5	6	60	5
550	34	222	7	19	231	6	19	231	6	30	80	4	5	100	6
500	43	218	6	19	232	6	19	232	6	29	78	3	15	185	9
450	45	224	8	23	238	6	23	238	6	27	71	3	15	212	12
400	55	228	8	24	255	5	25	255	5	25	57	6	23	214	14
350	63	228	9	27	263	5	21	263	5	21	40	9	30	210	15
300	76	232	10	35	250	7	35	250	7	15	13	11	37	202	14
250	95	235	12	27	253	7	27	253	7	14	323	11	40	194	11
200	106	241	13	31	300	5	31	300	5	19	291	10	42	185	8
175	115	245	14	40	288	5	40	288	5	22	283	9	39	180	6
150	134	249	15	46	287	3	46	287	3	21	286	7	35	178	5
125	156	253	16	52	277	4	52	277	4	18	288	6	27	179	4
100	187	256	19	58	282	5	58	282	5	16	284	5	21	179	3
80	223	259	20	63	271	5	63	271	5	19	283	5	17	184	3
60	282	262	24	77	271	7	77	271	7	29	276	5	19	202	4
50	325	261	28	87	271	7	87	271	7	41	272	4	27	211	5
40	385	263	33	100	272	8	100	272	8	50	271	4	32	204	6
30	477	264	37	122	265	9	122	265	9	56	271	5	28	184	8
20	651	263	49	160	259	12	160	259	12	62	269	7	23	137	8
15	820	263	78	200	269	19	200	269	19	84	258	8	18	100	13
10															

SFC	Height			Temperature			Northward Wind Component			Eastward Wind Component			
	P_a	A	α	ϵ	A	α	ϵ	A	α	ϵ	A	α	ϵ
Part A-6.—Sault Ste. Marie, Mich. (46°28' N., 84°22' W., 724 ft.)													
1000	0.30	339	0.05	32	236	34	22	311	3	92	210	8	
950	28	350	4	25	232	41	22	303	4	72	207	8	
900	21	306	5	10	208	7	22	285	3	45	200	6	
850	29	261	5	4	190	5	22	264	3	23	194	4	
800	30	252	5	2	188	5	22	264	3	23	194	4	
750	33	246	5	2	209	5	18	266	3	12	197	5	
700	38	243	6	2	228	5	13	298	2	7	221	7	
650	41	240	6	2	237	5	13	336	3	6	249	8	
600	44	240	6	2	244	3	15	367	4	6	279	8	
550	52	239	6	2	239	3	15	4	6	9	294	8	
500	52	239	7	2	237	3	15	357	6	11	294	8	
450	64	239	7	3	242	3	16	338	7	15	288	8	
400	68	243	8	3	249	4	20	316	7	18	283	8	
350	85	240	9	3	252	4	23	291	6	16	285	7	
300	97	240	10	3	243	4	26	263	6	10	302	7	
250	109	240	11	3	241	6	32	233	6	7	28	5	
200	120	239	12	2	258	5	38	212	8	15	65	3	
175	134	239	13	1	269	6	40	204	10	22	80	6	
150	138	240	12	2	264	5	37	211	9	22	94	10	
125	157	245	16	3	285	5	36	259	7	11	167	9	
100	173	248	18	4	285	4	36	267	6	11	210	6	
80	193	251	20	4	278	6	33	266	5	10	216	5	
60	214	255	22	5	276	8	30	267	4	10	179	5	
50	257	253	28	6	266	5	30	277	3	22	156	7	
40	295	253	34	7	268	6	34	287	2	38	156	8	
30	353	256	37	10	271	9	41	290	4	52	161	10	
20	508	255	83	12	266	18	52	290	12	64	176	19	
15													
10													

SFC	Height			Temperature			Northward Wind Component			Eastward Wind Component					
	p_0	A	α	ϵ	A	α	ϵ	A	α	ϵ	A	α	ϵ		
Part A-8.—Keflavik, Iceland (63°59' N., 22°38' W., 161 ft.)															
1000	0.13	159	0.04	84	247	14	84	247	14	8	107	3	20	198	7
950	9	170	4	66	247	13	66	247	13	7	135	3	19	180	6
900	1														

Table 3.—Continued

Height				Temperature			Northward Wind Component			Eastward Wind Component		
<i>p</i> ₀	<i>A</i>	<i>α</i>	<i>ε</i>	<i>A</i>	<i>α</i>	<i>ε</i>	<i>A</i>	<i>α</i>	<i>ε</i>	<i>A</i>	<i>α</i>	<i>ε</i>
Part A-9.—Thule, Greenland (76°31' N., 68°50' W., 194 ft.)												
SFC	0.07	48	0.05	71	235	17	11	196	4	30	233	7
1000	8	23	5	44	224	9	8	189	4	24	231	6
950	5	199	4	18	219	6	3	174	4	15	232	4
900	2	176	4	11	208	3	2	358	4	10	239	3
850	3	173	4	7	237	3	5	346	3	7	241	3
800	3	184	4	6	234	3	9	343	3	7	215	3
750	14	191	4	7	223	3	11	338	2	8	205	3
700	6	199	4	8	229	4	12	327	2	10	209	4
650	13	212	4	8	244	3	11	313	4	12	212	4
600	9	212	4	11	258	4	9	303	6	14	195	5
550	15	217	6	9	257	3	9	287	7	16	173	6
500	13	231	6	11	251	3	14	270	8	17	160	6
450	22	224	6	11	239	3	20	275	8	14	159	7
400	21	233	7	12	242	3	24	285	8	10	164	7
350	33	230	9	11	245	3	24	288	7	10	169	7
300	23	241	10	11	248	4	24	275	6	15	167	6
250	35	235	9	12	244	4	25	260	5	22	169	4
200	45	237	11	18	242	5	27	259	4	26	171	4
175	51	236	12	12	246	5	30	264	3	28	173	4
150	57	237	14	15	258	4	36	269	3	28	176	4
125	63	236	16	15	254	4	41	270	2	29	180	4
100	74	238	19	20	264	4	44	273	2	33	181	3
80	77	239	23	22	273	5	46	272	3	40	179	2
60	105	244	27	24	260	7	47	267	3	45	182	2
50	134	241	26	32	252	6	52	260	4	50	189	3
40	170	241	31	37	247	7	52	254	6	50	200	7
30	194	237	39	41	245	10	50	250	9	60	203	12
20	240	236	55	56	240	16	50	275	4	53	170	6
15	418	241	138	73	287	50						
10												

Height				Temperature			Northward Wind Component			Eastward Wind Component		
<i>p</i> ₀	<i>A</i>	<i>α</i>	<i>ε</i>	<i>A</i>	<i>α</i>	<i>ε</i>	<i>A</i>	<i>α</i>	<i>ε</i>	<i>A</i>	<i>α</i>	<i>ε</i>
Part B-2.—St. George, Bermuda (32°22' N., 64°40' W., 17 ft.)												
SFC	0.67	151	0.03	15	127	2	19	92	2	22	354	2
1000	68	151	3	6	89	2	24	92	2	24	352	2
950	59	152	4	1	38	2	30	90	2	28	351	3
900	58	149	3	1	308	2	31	92	2	23	349	3
850	58	148	3	4	66	4	3					
800	67	146	4	3	119	3	33	92	1	20	343	3
750	58	144	4	5	132	2	38	94	2	18	338	3
700	59	144	4	8	115	3	44	96	2	17	342	4
650	59	143	5	7	129	2	46	97	2	20	351	4
600	62	141	5	5	113	2	45	98	3	24	354	3
550	61	136	5	7	109	2	45	95	3	27	355	3
500	65	137	5	6	117	2	47	92	3	26	352	3
450	64	136	7	6	162	3	49	91	4	22	350	3
400	69	135	6	6	143	2	48	92	5	21	352	2
350	71	134	7	3	158	2	41	91	5	21	2	4
300	73	132	7	4	129	3	33	82	5	22	20	7
250	76	131	8	6	146	3	31	70	4	24	33	8
200	80	129	9	6	136	3	31	67	3	24	40	8
175	83	127	10	10	112	3	29	76	3	20	34	6
150	87	124	10	10	140	4	25	93	4	14	16	5
125	92	126	11	15	160	5	26	105	4	11	347	3
100	101	126	12	16	147	4	30	94	3	12	336	3
80	110	126	13	18	116	4	34	82	2	15	338	6
60	125	123	15	14	159	5	36	74	2	20	334	8
50	129	121	16	18	111	5	37	78	3	26	323	9
40	143	118	19	21	117	6	43	79	4	32	308	10
30	162	119	23	20	142	9	49	75	4	37	296	11
20	154	123	32	13	170	11	50	65	4	39	292	12
15	116	122	31	8	276	21	42	56	4	36	313	12
10												

Height				Temperature			Northward Wind Component			Eastward Wind Component		
<i>p</i> ₀	<i>A</i>	<i>α</i>	<i>ε</i>	<i>A</i>	<i>α</i>	<i>ε</i>	<i>A</i>	<i>α</i>	<i>ε</i>	<i>A</i>	<i>α</i>	<i>ε</i>
Part B-1.—Eglin Air Force Base, Valparaiso, Fla. (30°29' N., 86°31' W.)												
SFC	0.54	149	0.04	75	91	10	39	64	4	31	12	2
1000	48	146	3	56	73	7	39	63	4	27	359	2
950	40	142	3	23	35	3	39	65	4	24	338	3
900	48	134	4	10	32	3	38	72	5	25	331	3
850	47	132	4	6	9	2	37	82	6	27	332	3
800	47	131	4	1	43	2	39	88	5	29	337	3
750	45	119	6	4	105	3	38	88	5	30	344	3
700	48	128	4	4	134	3	38	92	5	33	354	3
650	47	125	4	2	107	3	36	94	6	36	354	3
600	50	126	4	5	93	2	32	95	6	35	13	3
550	51	124	5	3	69	2	27	88	6	32	30	3
500	61	140	11	3	80	3	23	78	5	34	42	3
450	50	122	6	4	101	3	18	72	4	33	44	4
400	54	118	4	4	134	3	13	82	4	27	35	4
350	56	117	5	4	142	3	14	103	4	20	27	5
300	57	115	6	3	136	2	19	115	4	18	22	5
250	58	114	6	2	144	3	24	116	5	20	18	5
200	59	115	7	9	181	3	28	114	6	19	22	3
175	61	116	8	9	150	3	31	104	7	14	37	3
150	64	115	9	4	124	4	33	89	6	11	54	2
125	67	114	9	13	160	3	37	76	5	12	29	2
100	74	118	10	8	161	3	42	65	4	20	4	1
80	82	121	11	4	184	5	48	59	4	31	358	3
60	86	120	14	8	173	7	52	56	5	42	338	3
50	90	119	17	10	144	7	53	55	4	50	359	2
40	96	120	19	5	167	6	55	57	4	50	356	3
30	104	118	21	5	105	6	61	59	3	48	335	9
20	119	111	26	19	94	9	65	62	6	54	308	17
15	117	98	38	22	112	11	71	76	4	105	255	72
10	212	47	114	35	60	16						

Height				Temperature			Northward Wind Component			Eastward Wind Component		
<i>p</i> ₀	<i>A</i>	<i>α</i>	<i>ε</i>	<i>A</i>	<i>α</i>	<i>ε</i>	<i>A</i>	<i>α</i>	<i>ε</i>	<i>A</i>	<i>α</i>	<i>ε</i>
Part B-3.—Fort Worth, Tex. (32°50' N., 97°3' W., 576 ft.)												
SFC	0.85	152	0.04	89	49	12	13	72	2	18	36	3
1000	75	152	3	74	54	20	16	74	1	17	21	3
950	68	145	4	52	3	5	21	79	4	16	12	3
900	64	142	3	31	341	8	26	82	6	14	14	3
850	60	140	3	15	348	5	31	85	6	19	13	2
800	58	137	4	8	23	4	36	82	5	26	3	3
750	58	134	4	5	39	3	40	78	2	31	352	3
700	57	133	4	5	28	3	44	74	2	34	345	4
650	56	128	5	5	36	3	45	68	1	32	342	5
600	57	130	4	4	97	2	45	62	1	30	340	5
550	54	126										

Table 3.—Continued

SFC	Height			Temperature			Northward Wind Component			Eastward Wind Component			
	<i>p</i> ₀	<i>A</i>	<i>α</i>	<i>ε</i>	<i>A</i>	<i>α</i>	<i>ε</i>	<i>A</i>	<i>α</i>	<i>ε</i>	<i>A</i>	<i>α</i>	<i>ε</i>
Part B-4—Osan, Korea (37°6' N., 127°2' E.)													
1000	0.54	147	0.05	75	77	7	4	150	4	25	359	3	
950	44	143	4	56	59	7	11	114	2	23	355	3	
900	45	134	6	20	35	4	3	19	106	2	20	348	2
850	43	132	4	3	13	3	19	106	2	20	348	2	
	44	131	4	5	152	3	22	103	1	20	344	2	
800	45	130	4	9	156	3	24	95	2	23	350	2	
750	43	128	4	9	161	3	26	83	3	28	357	2	
700	45	131	5	8	178	3	29	77	3	33	2	2	
650	46	128	6	4	255	3	34	74	3	34	3	3	
600	50	130	6	1	301	3	40	72	3	36	5	5	
550	47	129	8	5	136	3	45	69	3	40	2	7	
500	53	128	5	4	129	3	50	71	4	45	356	7	
450	50	126	6	5	100	3	56	76	5	50	345	8	
400	54	124	6	7	113	3	66	78	6	55	335	8	
350	61	122	6	7	144	3	71	78	7	56	330	8	
300	65	122	7	10	134	4	65	80	8	50	328	7	
250	72	122	7	14	132	3	51	87	8	35	324	5	
200	81	121	8	6	123	3	35	92	7	21	309	6	
175	85	120	8	11	127	4	24	82	6	11	284	10	
150	91	119	9	15	138	4	26	55	5	2	352	14	
125	97	119	11	16	132	5	36	45	4	16	76	17	
100	103	120	12	14	140	4	44	45	4	34	82	19	
80	110	121	13	11	153	4	49	51	3	49	82	22	
60	122	121	16	6	96	6	49	58	3	53	78	24	
50	123	117	17	4	275	6	48	63	4	49	72	24	
40	126	113	20	5	109	7	40	60	3	38	62	21	
30	134	112	26	11	91	7	35	49	3	27	39	19	
20	114	111	44	6	171	14	29	29	6	45	318	24	
15	88	98	67	18	287	17	24	9	7	94	300	29	
10	92	181	50	61	235	21	23	350	8	137	291	50	

SFC	Height			Temperature			Northward Wind Component			Eastward Wind Component			
	<i>p</i> ₀	<i>A</i>	<i>α</i>	<i>ε</i>	<i>A</i>	<i>α</i>	<i>ε</i>	<i>A</i>	<i>α</i>	<i>ε</i>	<i>A</i>	<i>α</i>	<i>ε</i>
Part B-6—Sault Ste. Marie, Mich. (46°28' N., 84°22' W., 724 ft.)													
1000	0.32	186	0.03	67	66	8	19	128	4	25	13	3	
950	26	184	2	63	103	24	24	125	4	27	359	2	
900	24	173	3	30	47	4	24	119	4	32	350	2	
850	20	165	2	10	21	4	27	119	4	32	350	2	
	19	162	2	2	56	4	28	107	4	38	351	2	
800	20	161	2	4	116	4	29	90	5	42	353	3	
750	22	158	2	4	117	3	36	79	6	44	354	3	
700	21	156	2	0	---	2	39	75	5	42	356	4	
650	21	145	4	2	19	2	39	77	5	37	357	4	
600	20	154	3	2	0	2	37	84	4	35	357	4	
550	20	157	5	4	50	2	35	90	4	35	358	4	
500	19	147	4	3	35	3	33	90	3	39	2	4	
450	15	150	6	6	105	2	30	89	3	44	5	4	
400	22	136	5	8	84	2	27	94	4	45	5	3	
350	24	133	5	5	104	3	25	104	5	41	4	4	
300	25	126	5	3	93	4	23	102	5	30	2	5	
250	25	119	6	8	201	3	21	88	4	19	358	6	
200	30	125	6	11	131	4	22	69	4	14	345	5	
175	33	123	7	8	107	4	26	62	3	19	357	4	
150	37	119	7	7	146	5	24	60	3	30	338	3	
125	39	123	9	2	190	4	43	64	4	38	344	3	
100	45	119	11	8	101	6	50	72	4	42	347	3	
80	45	105	13	3	95	4	54	80	4	43	348	3	
60	49	102	15	10	49	7	52	83	4	46	345	3	
50	49	102	12	7	56	6	52	83	4	46	345	4	
40	54	102	24	15	112	8	57	76	4	42	350	4	
30	70	111	27	12	150	10	68	69	4	40	355	5	
20	72	93	40	5	72	13	84	65	7	43	352	10	
15													
10													

SFC	Height			Temperature			Northward Wind Component			Eastward Wind Component			
	<i>p</i> ₀	<i>A</i>	<i>α</i>	<i>ε</i>	<i>A</i>	<i>α</i>	<i>ε</i>	<i>A</i>	<i>α</i>	<i>ε</i>	<i>A</i>	<i>α</i>	<i>ε</i>
Part B-5—Terceira, Azores (38°45' N., 27°5' W., 177 ft.)													
1000	0.52	156	0.03	30	91	3	23	98	3	11	14	3	
950	45	153	3	16	78	3	25	88	3	13	2	3	
900	45	150	3	9	68	3	27	77	2	15	353	3	
850	44	149	3	2	27	3	28	67	2	17	347	2	
800	44	148	3	5	8	4	26	65	2	17	347	2	
750	44	140	4	4	22	4	25	73	2	19	348	3	
700	43	144	3	3	59	3	23	88	2	20	347	3	
650	50	136	3	4	32	2	21	89	2	21	346	3	
600	45	141	4	7	54	2	16	76	2	22	348	3	
550	49	134	5	6	40	2	16	54	3	25	348	3	
500	45	134	4	4	71	2	17	43	4	26	347	4	
450	39	131	7	1	112	3	17	38	4	26	338	3	
400	40	126	5	3	142	3	18	30	5	31	341	3	
350	39	124	6	0	---	2	17	25	5	36	342	3	
300	40	120	6	7	123	5	16	23	5	37	336	3	
250	43	117	7	3	92	3	16	28	3	36	331	3	
200	45	112	8	5	90	3	20	39	2	36	327	2	
175	47	113	8	8	132	3	25	51	2	37	331	2	
150	51	113	8	9	120	4	28	58	1	36	330	2	
125	59	106	9	6	134	3	29	63	2	38	329	3	
100	65	105	9	10	128	4	28	67	1	37	327	4	
80	72	106	10	16	133	3	29	67	2	37	326	3	
60	80	108	13	18	146	3	33	61	3	36	318	3	
50	94	112	11	15	125	4	41	59	3	39	317	4	
40	104	110	13	19	141	4	51	63	3	46	326	5	
30	115	112	14	10	143	5	54	72	3	54	339	5	
20	125	109	22	14	95	8	54	79	4	57	347	3	
15	120	101	29	13	78	9	50	76	6	50	348	4	
10	102	90	55	42	74	19	47	59	8	39	342	8	

SFC	Height			Temperature			Northward Wind Component			Eastward Wind Component			
	<i>p</i> ₀	<i>A</i>	<i>α</i>	<i>ε</i>	<i>A</i>	<i>α</i>	<i>ε</i>	<i>A</i>	<i>α</i>	<i>ε</i>	<i>A</i>	<i>α</i>	<i>ε</i>
Part B-7—Stephenville, Newfoundland (48°32' N., 58°33' W., 44 ft.)													
1000	0.25	190	0.04	34	92	6	13	126	3	25	35	3	
950	18	195	3	29	78	5	16	104	3	22	29	2	
900	18	193	4	18	62	4	21	86	3	15	19	3	
850	18	170	3	7	66	4	26	77	2	9	1	3	
800	18	166	3	2	64	4	30	76	3	11	344	3	
750	21	161	4	3	81	3	31	75	4	22	348	3	
700	18	163	3	4	27								

Table 3.—Continued

Height				Temperature			Northward Wind Component			Eastward Wind Component		
p_0	A	α	ϵ	A	α	ϵ	A	α	ϵ	A	α	ϵ
Part B-8—Keflavik, Iceland (63°59' N., 22°38' W., 161 ft.)												
SFC	0.16	156	0.04	6	64	3	16	119	3	17	357	6
1000	13	152	3	6	6	3	16	123	3	17	6	5
950	19	118	5	3	16	3	12	122	3	16	8	5
900	13	147	3	2	312	3	9	102	4	16	3	4
850	12	182	6	2	260	3	8	76	4	18	351	4
800	13	150	3	3	243	3	8	72	4	18	344	3
750	13	162	4	6	222	2	9	73	4	20	337	3
700	13	157	3	2	194	2	11	66	4	21	332	4
650	16	160	5	2	204	2	14	56	6	23	330	5
600	14	154	4	3	188	3	15	47	7	23	332	6
550	12	164	4	6	215	2	17	43	7	21	346	6
500	16	158	4	3	200	3	23	52	6	24	7	7
450	15	141	6	3	183	3	29	63	4	28	16	7
400	17	164	6	2	138	3	31	68	4	24	14	7
350	17	168	6	1	32	3	30	64	4	17	0	7
300	17	164	7	4	76	3	27	48	3	15	343	6
250	17	156	7	3	43	4	29	38	2	21	335	5
200	16	147	8	6	74	3	27	39	2	24	330	3
175	17	136	8	6	82	3	26	50	2	22	314	3
150	19	127	9	5	151	3	25	62	2	21	308	2
125	21	129	10	3	180	3	27	62	2	21	318	2
100	23	135	11	7	135	4	27	58	2	22	339	2
80	25	128	11	5	71	4	27	53	2	23	356	2
60	24	121	14	4	120	4	27	64	2	28	358	2
50	26	141	13	1	42	4	33	81	3	34	351	3
40	27	147	14	5	47	4	37	84	5	37	341	6
30	36	133	19	7	114	6	45	76	7	38	340	8
20	27	134	26	8	71	7	72	62	11	29	350	8
15	50	130	37	9	16	10	72	62	11	29	350	8
10	10	314	19	99	295	41	95	57	19	35	4	13

Height				Temperature			Northward Wind Component			Eastward Wind Component		
p_0	A	α	ϵ	A	α	ϵ	A	α	ϵ	A	α	ϵ
Part B-9—Thule, Greenland (76°31' N., 68°50' W., 194 ft.)												
SFC	0.16	189	0.03	6	11	4	3	111	2	6	273	2
1000	15	212	4	2	291	5	4	2	5	77	2	1
950	12	177	3	4	2	2	3	8	2	8	57	2
900	12	187	2	3	8	2	12	41	2	11	284	2
850	12	186	2	0	-----	3	8	41	2	11	284	2
800	12	188	3	4	231	2	18	38	2	12	278	2
750	11	218	4	3	3	2	20	41	2	12	293	2
700	11	188	3	1	118	2	18	44	2	13	320	2
650	9	220	4	2	219	2	15	45	3	16	336	2
600	12	183	3	3	254	2	12	44	3	18	339	2
550	12	190	5	1	287	2	11	41	2	19	332	2
500	11	186	4	3	3	2	9	40	2	18	337	3
450	5	213	5	3	25	2	7	23	3	18	345	3
400	9	187	4	1	275	2	8	26	3	21	352	3
350	7	238	6	3	351	2	9	41	3	21	341	2
300	14	173	8.	2	18	3	11	46	3	18	330	3
250	7	210	7	7	261	4	10	49	3	13	313	2
200	8	216	8	5	200	3	8	42	4	9	306	2
175	9	219	8	3	244	2	9	56	3	8	297	1
150	11	212	9	2	262	2	12	44	3	11	306	2
125	11	225	9	3	208	3	16	35	2	15	312	1
100	14	208	12	2	281	3	20	27	2	21	319	2
80	9	198	14	1	304	3	21	32	3	28	324	3
60	11	172	17	1	74	4	20	39	2	33	326	3
50	14	191	18	2	97	4	19	49	2	33	327	4
40	10	120	22	2	68	5	18	63	2	25	332	4
30	25	101	31	9	127	8	14	72	2	15	351	5
20	26	101	42	12	267	9	8	66	4	17	26	8
15	57	338	40	34	311	20	28	294	5	14	273	8

APPENDIX C

If the coefficient of eddy exchange of momentum, K_m , is assumed independent of height, and the undisturbed atmosphere is considered to be at rest, the equations of motion for the tidal perturbations become

$$\frac{\partial u}{\partial t} - 2\omega v \cos \theta + \frac{1}{a} \frac{\partial}{\partial \theta} \left(\frac{\delta p}{\rho_0} \right) - K_m \frac{\partial^2 u}{\partial z^2} = 0 \quad (75)$$

$$\frac{\partial v}{\partial t} + 2\omega u \cos \theta + \frac{1}{a \sin \theta} \frac{\partial}{\partial \phi} \left(\frac{\delta p}{\rho_0} \right) - K_m \frac{\partial^2 v}{\partial z^2} = 0 \quad (76)$$

when the tidal potential is neglected. Here, K_m is the mean value of the exchange coefficient, which is known to have a pronounced time variation. Although the equations as written above are consistent with perturbation theory, in which the products of time-variable quantities are neglected, and with the assumption that the undisturbed atmosphere is at rest, they probably represent at best a rather crude approximation to reality. Thus the model to be described can yield only a rough estimate of the surface stress components.

At the lower boundary of the friction layer, the wind shear is assumed to be parallel to the wind itself; hence

$$u_a = k \left(\frac{\partial u}{\partial z} \right)_a, \quad v_a = k \left(\frac{\partial v}{\partial z} \right)_a \quad (77)$$

the wind being continuous at the boundary $z=a$. The constant k may be thought of as a coefficient of surface friction, and can be shown to be

$$k = (z_a + z_0) \ln \frac{z_a + z_0}{z_0} \quad (78)$$

where z_0 is the roughness parameter. We shall assume that z_a is the height of the anemometer level and in the following computations the height will be counted above this level so that $z_a=0$. At some upper level, marking the top of the friction layer, the eddy friction terms are assumed to be negligibly small. Since equations (75) and (76) are linear, solutions for u and v may be represented as a sum of solutions

$$\begin{aligned} u &= u_p + u_f \\ v &= v_p + v_f. \end{aligned} \quad (79)$$

Here, u_p and v_p are taken to be functions of $\delta p/\rho_0$ alone, while u_f and v_f may be considered perturbations about u_p and v_p , respectively. It follows that u_p and v_p at the upper boundary, where the eddy friction terms are negligible, must satisfy the equations

$$\frac{\partial u_p}{\partial t} - 2\omega v_p \cos \theta + \frac{1}{a} \frac{\partial}{\partial \theta} \left(\frac{\delta p}{\rho_0} \right) = 0 \quad (80)$$

TABLE 4.—Amplitude (*A*) and phase (α), of the computed diurnal (Part A) and semidiurnal (Part B) variations in isobaric height, 10^{-1} m. at nine rawinsonde stations, for period July 1956 to June 1958. The values were computed from the observed wind variations

<i>p</i> ₀ (mb.)	Valparaiso		Bermuda		Ft. Worth		Osan		Azores		S. Ste. Marie		Stephenville		Keflavik		Thule	
	<i>A</i>	α	<i>A</i>	α	<i>A</i>	α	<i>A</i>	α	<i>A</i>	α	<i>A</i>	α	<i>A</i>	α	<i>A</i>	α	<i>A</i>	α
Part A.—Diurnal Variations																		
SFC.....	246	95	58	68	132	126	146	29	45	232	199	25	125	76	71	18	51	75
950.....	170	88	39	58	98	124	99	27	64	207	133	22	76	99	63	18	40	69
900.....	100	62	26	20	81	133	55	29	87	194	42	32	73	153	53	23	22	60
850.....	93	40	30	347	89	141	41	58	94	198	43	137	81	166	42	32	8	45
800.....	97	51	29	332	108	146	63	77	75	207	54	161	54	153	40	53	5	286
750.....	106	71	17	322	97	150	71	93	60	233	39	200	15	59	41	61	15	271
700.....	101	76	9	123	89	170	80	108	54	253	45	245	60	354	51	73	19	265
650.....	87	74	45	110	96	198	81	118	70	262	53	263	98	344	60	76	16	255
600.....	53	78	66	120	129	217	76	116	81	270	47	263	126	342	70	75	10	236
550.....	22	114	69	135	151	229	68	118	107	277	44	246	145	345	66	65	7	257
500.....	19	205	72	168	170	235	56	130	116	271	50	208	166	350	57	52	8	262
450.....	27	253	79	184	183	236	26	119	115	254	80	187	160	354	44	43	13	210
400.....	23	259	87	187	200	228	54	36	93	222	116	174	158	351	33	28	30	199
350.....	27	265	99	188	226	213	117	45	70	197	147	163	150	348	22	352	42	203
300.....	33	265	135	191	245	197	175	72	39	171	161	151	126	347	17	304	43	205
250.....	42	265	197	203	242	181	226	94	21	120	160	136	86	347	9	241	35	194
200.....	42	237	260	213	211	166	234	106	37	122	138	130	51	337	8	127	30	171
175.....	37	207	307	223	166	154	189	106	61	121	113	137	40	305	7	111	30	168
150.....	32	191	317	228	116	144	137	81	62	108	115	160	33	293	5	204	34	176
125.....	15	175	287	233	83	139	145	52	52	69	138	169	28	276	25	184	46	181
100.....	9	183	237	238	84	142	137	45	48	45	141	169	21	248	44	159	56	181
80.....	21	187	183	248	123	143	75	59	32	68	132	166	40	206	58	148	57	184
60.....	39	181	133	253	141	159	45	128	38	150	110	176	82	175	62	152	54	184
50.....	40	159	68	247	122	173	99	158	72	162	88	212	127	162	64	166	51	171
40.....	36	136	31	186	93	164	148	157	80	154	104	246	148	165	83	176	63	154
30.....	38	192	35	159	123	122	171	156	93	158	123	260	172	180	120	171	73	134
20.....	152	221	43	213	258	103	150	128	126	178	101	256	244	190	153	162	74	121
15.....	285	220	109	265			280	106	203	197			377	176	176	174	20	218
10.....	488	209					499	105	266	207					128	195		
Part B.—Semidiurnal Variations																		
SFC.....	82	230	46	167	62	238	89	173	12	346	45	167	49	215	19	118	9	70
950.....	50	224	44	159	46	228	65	164	10	337	53	140	34	226	16	129	7	70
900.....	19	171	41	158	27	232	44	140	10	317	66	134	20	253	16	152	6	64
850.....	31	121	29	139	21	273	39	124	12	257	70	146	35	336	17	174	6	13
800.....	46	117	26	105	23	251	38	149	14	238	69	166	36	347	23	174	10	348
750.....	48	121	37	65	31	208	47	182	15	186	58	182	7	308	22	165	10	334
700.....	50	141	41	50	39	181	63	198	23	142	49	197	51	189	24	153	5	298
650.....	58	164	30	55	40	168	61	208	32	146	34	204	103	186	22	149	7	218
600.....	74	183	23	95	30	174	63	219	44	170	27	188	133	187	22	153	10	192
550.....	78	200	20	125	26	194	70	217	60	182	31	176	137	188	21	171	11	175
500.....	90	229	19	99	19	208	68	202	69	186	50	185	130	191	25	211	12	178
450.....	116	242	26	46	16	186	62	165	66	175	72	190	113	197	36	243	17	187
400.....	120	240	26	41	13	139	69	128	86	179	83	186	103	208	42	258	19	193
350.....	92	227	4	333	25	114	78	110	110	178	74	176	100	218	35	278	15	179
300.....	54	214	42	254	32	100	76	100	112	170	45	168	98	217	28	300	9	167
250.....	35	198	77	257	36	105	73	83	104	162	12	178	91	213	26	288	4	115
200.....	35	188	89	262	39	122	70	64	91	156	9	302	92	214	25	257	2	86
175.....	18	197	59	265	59	145	54	35	81	158	6	232	102	216	19	235	5	47
150.....	25	313	12	279	82	154	52	322	69	152	22	190	98	208	5	34	2	10
125.....	57	320	27	67	86	156	125	290	73	145	29	199	89	189	20	40	2	255
100.....	52	307	30	51	79	156	205	285	74	138	21	197	75	167	14	21	9	206
80.....	43	265	19	35	97	149	259	283	72	137	14	142	64	162	11	273	14	183
60.....	63	227	12	77	109	160	262	282	61	122	32	132	30	220	28	254	18	167
50.....	100	213	46	96	111	153	227	280	54	114	33	134	58	262	24	238	16	156
40.....	128	208	86	83	110	132	172	274	55	132	9	239	67	250	8	166	9	150
30.....	115	204	112	70	102	103	117	261	74	156	49	295	70	212	20	58	3	222
20.....	70	166	104	69	89	63	110	149	85	164	76	303	89	177	33	2	15	230
15.....	113	98	58	113			303	124	69	173			106	165	79	319	29	173
10.....	457	56					474	114	45	194					128	307		

$$\frac{\partial v_p}{\partial t} + 2\omega u_p \cos \theta + \frac{1}{a \sin \theta} \frac{\partial}{\partial p} \left(\frac{\delta p}{\rho_0} \right) = 0. \quad (81)$$

In [7], it was shown that the variation of $\delta p/\rho_0$ with height is comparatively small, so that equations (80) and (81) may be assumed to hold true not only at the upper boundary but throughout the friction layer. Thus the solution for u_p and v_p is the same as for u and v in equations (34) and (35) when the tidal potential and frictional terms are neglected.

Since u_r and v_r are proportional to $e^{i\omega t}$, and $f=0.99727 \approx$

1, these components of the wind must satisfy the equations

$$u_f = -\frac{K_m}{2\omega \sin^2 \theta} \left(\cos \theta \frac{\partial^2 u_f}{\partial z^2} + i \frac{\partial^2 u_f}{\partial z^2} \right) \quad (82)$$

$$v_f = \frac{K_m}{2\omega \sin^2 \theta} \left(\cos \theta \frac{\partial^2 v_f}{\partial z^2} - i \frac{\partial^2 v_f}{\partial z^2} \right). \quad (83)$$

A solution satisfying the above equations is

$$v_r = A e^{-bz} \sin (2\omega t + \alpha - bz) \quad (84)$$

$$u_r = -B e^{-bz} \cos (2\omega t + \alpha - bz) \quad (85)$$

provided

$$b = \left(\frac{\omega}{K_m} \right)^{1/2} \left(\frac{A}{A+B \cos \theta} \right)^{1/2} \sin \theta \quad (86)$$

and

$$\left(\frac{A}{A+B \cos \theta} \right)^{1/2} = \left(\frac{B}{B+A \cos \theta} \right)^{1/2} \quad (87)$$

The constants A , B , and α can be determined from the lower boundary condition (equation (77)) in the following way.

Equation (79) becomes, at the anemometer level,

$$\begin{aligned} u_a &= u_p + (u_f)_a \\ v_a &= v_p + (v_f)_a \end{aligned} \quad (88)$$

From the condition $z=0$ at z_a and equations (84) and (85), it follows that

$$(v_f)_a = A \sin (2\omega t + \alpha) \quad (89)$$

$$(u_f)_a = -B \cos (2\omega t + \alpha). \quad (90)$$

By carrying out the differentiation with respect to z in equation (77), it can be shown that

$$v_a = \sqrt{2} b A k \sin (2\omega t + \alpha + 225^\circ) \quad (91)$$

$$u_a = -\sqrt{2} b B k \cos (2\omega t + \alpha + 225^\circ). \quad (92)$$

Hence the second part of equation (88) becomes

$$\sqrt{2} b A k \sin (2\omega t + \alpha - 135^\circ) = v_p + A \sin (2\omega t + \alpha) \quad (93)$$

and a similar equation holds for the u component. Equation (93) is sufficient to obtain b .

In figure 9, β is the phase angle of v_p , which is observed to be about 338° . The vectors $(v_f)_a$ and v_a are drawn so that within the triangle DEF, angle E = 135° , a condition necessary to satisfy equation (93). The magnitudes of the vectors v_a and $(v_f)_a$ are $\sqrt{2} b A k$ and A , respectively, the amplitudes of the harmonic functions in equation (93). It is evident from figure 9 that

$$\alpha = \beta + 135^\circ + D \quad (94)$$

and also that v_f is parallel to v_p at some height h where

$$bh = 2\pi + \alpha - \beta \quad (95)$$

The height h is approximately equal to the depth of the frictional layer.

It follows from the law of sines and from figure 9 that

$$A = \sqrt{2} V_p \sin D \quad (96)$$

where V_p is the amplitude of v_p , and by analogy that

$$B = \sqrt{2} U_p \sin D \quad (97)$$

where U_p is the amplitude of u_p .

The surface stress components are found by multiplying

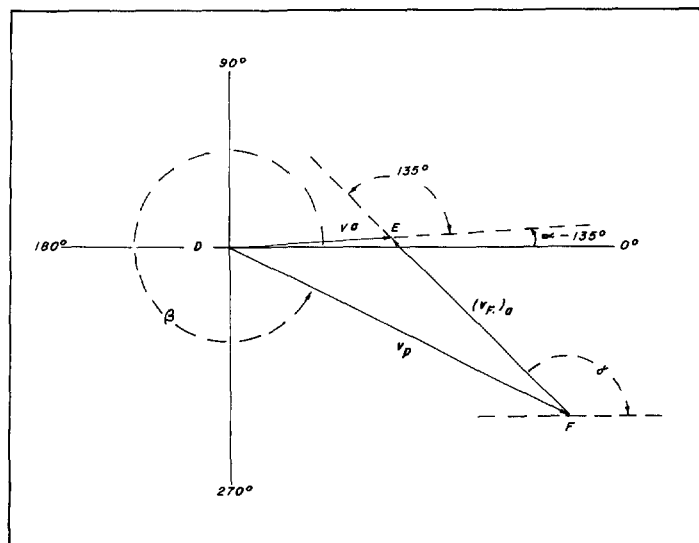


FIGURE 9.—Determination of constants α and A .

equations (91) and (92) by $\rho_0 K_m / k$. Then substituting for α , b , K_m , A , and B from equations (94), (95), (86), (96), and (97), respectively, we find that

$$\delta \tau_\phi(0) = \frac{8\rho_0\omega V_p^2 \sin^2 \theta h \sin D}{V_p + U_p \cos \theta 3\pi + 4D} \sin (2\omega t + \beta + D) \quad (98)$$

$$\delta \tau_\theta(0) = \frac{-8\rho_0\omega U_p^2 \sin^2 \theta h \sin D}{U_p + V_p \cos \theta 3\pi + 4D} \cos (2\omega t + \beta + D). \quad (99)$$

Using the law of sines and figure 9 one can show that

$$D = \cot^{-1} (1 + 2kb) \quad (100)$$

whence it follows that D may vary between 0° and 45° .

The amplitudes V_p and U_p of the pressure dependent components of the wind can be estimated from equations (34) and (35) and from the observed pressure distribution. Cross-differentiation of (34) and (35) yields an equation in the vorticity and the divergence. This equation can be integrated with respect to height to obtain the vorticity of the mean wind in terms of $\delta p(0)$. The mean wind in the layer is a pressure-weighted mean. By integrating the continuity equation (22) through the atmospheric layer, and assuming the boundary conditions $\rho_0 w = 0$ at $z=0$ and $z=\infty$, we then eliminate \bar{v} between the two equations to find

$$\frac{d^2 \bar{u}}{d\theta^2} - 3 \cot \theta \frac{d\bar{u}}{d\theta} - 3 \csc^2 \theta \bar{u} = \frac{-ai}{p_0(0)} \left(\cot \theta + \frac{d}{d\theta} \right) \delta p(0). \quad (101)$$

Since the homogeneous part of equation (101) has an elementary solution, the complete solution can be found by the method of variation of parameters. When the boundary conditions $\bar{u} = 0$ at $\theta = 0$ and $\theta = 90^\circ$ are assumed, and $\delta p(0) = 1.20 \text{ mb.} \sin^2 \theta \sin (2\omega t + 138^\circ)$, \bar{u} can be evaluated. This component of the mean wind is then sub-

stituted into the integrated form of the continuity equation to obtain v . In this way, it is found that the mean wind components, in cm. sec.⁻¹, are

$$\bar{v} = (49.0 \sin \theta - 13.8 \sin^3 \theta - 14.1 \sin^5 \theta) \sin (2\omega t + 338^\circ) \quad (102)$$

$$\bar{u} = (49.0 \sin \theta \cos \theta + 18.8 \sin^3 \theta \cos \theta) \sin (2\omega t + 248^\circ). \quad (103)$$

Since the frictional effect should be small when the wind is integrated through the total atmospheric layer, it is assumed that the amplitudes of \bar{v} and \bar{u} are approximately equal to V_p and U_p .

ACKNOWLEDGMENTS

The authors express their appreciation to Mr. William P. Townshend for programing assistance and to Mr. James E. Caskey, Jr., for many helpful discussions concerning the mathematical development.

REFERENCES

1. S. T. Butler, and K. A. Small, "The Excitation of Atmospheric Oscillations," *Proceedings of the Royal Society of London, Ser. A*, vol. 274, 1963, pp. 91-121.
2. S. Chapman, "Atmospheric Tides and Oscillations," *Compendium of Meteorology*, American Meteorological Society, Boston, 1951, pp. 510-530.
3. M. A. Estoque, "A Preliminary Report on a Boundary Layer Numerical Experiment," *GRD Research Notes No. 20*, Air Force Cambridge Research Laboratories, Bedford, Mass., 1959, 29 pp.
4. F. G. Finger, M. F. Harris, and S. Teweles, "Diurnal Variation of Wind, Pressure, and Temperature in the Stratosphere," *Journal of Applied Meteorology*, vol. 4, No. 5, Oct. 1965, pp. 632-635.
5. J. S. A. Green, "Atmospheric Tidal Oscillations: An Analysis of the Mechanics," *Proceedings of the Royal Society of London, Ser. A*, vol. 288, 1965, pp. 479-492.
6. M. F. Harris, "Diurnal and Semidiurnal Variations of Wind, Pressure and Temperature in the Troposphere at Washington, D.C.," *Journal of Geophysical Research*, vol. 64, No. 8, Aug. 1959, pp. 983-995.
7. M. F. Harris, "Semidiurnal Tidal Motions in the Friction Layer," *Monthly Weather Review*, vol. 91, Nos. 10-12, Oct.-Dec. 1963, pp. 557-565.
8. M. F. Harris, F. G. Finger, and S. Teweles, "Diurnal Variation of Wind, Pressure, and Temperature in the Troposphere and Stratosphere over the Azores," *Journal of Atmospheric Sciences*, vol. 19, No. 2, Mar. 1962, pp. 136-149.
9. B. Haurwitz, "The Geographical Distribution of the Solar Semidiurnal Pressure Oscillation," *Meteorological Papers*, vol. 2, No. 5, New York University, 1956, pp. 1-36.
10. B. Haurwitz, "Atmospheric Tides," *Science*, vol. 144, No. 3625, 1964, pp. 1415-1422.
11. B. Haurwitz and F. Möller, "The Semidiurnal Air-Temperature Variation and the Solar Air Tide," *Archiv für Meteorologie, Geophysik, und Bioklimatologie, Ser. A*, vol. 8, 1955, pp. 332-350.
12. D. H. Johnson, "Tidal Oscillations of the Lower Stratosphere," *Quarterly Journal of the Royal Meteorological Society*, vol. 81, 1955, pp. 1-8.
13. M. Siebert, "Atmospheric Tides," *Advances in Geophysics*, vol. 7, Academic Press, New York, 1961, pp. 105-187.

[Received April 7, 1966; revised May 19, 1966]